JPn

Neuroscience

The Journal of Physiology

Mapping the cellular electrophysiology of rat sympathetic preganglionic neurones to their roles in cardiorespiratory reflex integration: a whole cell recording study *in situ*

Alexey O. Stalbovskiy[1], Linford J. B. Briant[1,3], Julian F. R. Paton[1] and Anthony E. Pickering[1,2]

[1]*School of Physiology & Pharmacology, Bristol Heart Institute, Medical Sciences Building, University Walk, University of Bristol, Bristol BS8 1TD, UK*
[2]*Department of Anaesthesia, University Hospitals Bristol, Bristol BS2 8HW, UK*
[3]*Department of Engineering Mathematics, Merchant Venturers Building, Woodland Road, University of Bristol, Bristol BS8 1UB, UK*

Key points

- Sympathetic preganglionic neurones (SPNs) gatekeep the activity flowing from the CNS to the periphery and their intrinsic properties are believed to play an important integrative role in determining the firing patterns.
- Previous cell recording studies have explored the electrophysiological characteristics of SPNs but until now it has not been possible to link this knowledge to their roles in cardiorespiratory integration.
- We used the working heart–brainstem preparation to make whole-cell patch clamp recordings from thoracic SPNs ($n = 98$).
- The SPNs were classified into muscle vasoconstrictor-like (MVC_{like}, 39%) and cutaneous vasoconstrictor-like (CVC_{like}, 28%) on the basis of their dichotomous responses to cardio-respiratory reflex activation.
- The MVC_{like} SPNs have higher baseline firing frequencies and distinctive intrinsic properties. Their firing is driven by a barrage of excitatory synaptic potentials with both tonic and respiratory modulated components.
- The CVC_{like} SPNs show stereotyped rhythmical membrane potential oscillations that underpin their action potential discharge.
- We propose that these striking differences in the intrinsic properties of the classes of SPNs are likely to play an important role in patterning the sympathetic outflow.

Abstract Sympathetic preganglionic neurones (SPNs) convey sympathetic activity flowing from the CNS to the periphery to reach the target organs. Although previous *in vivo* and *in vitro* cell recording studies have explored their electrophysiological characteristics, it has not been possible to relate these characteristics to their roles in cardiorespiratory reflex integration. We used the working heart–brainstem preparation to make whole cell patch clamp recordings from T3–4 SPNs ($n = 98$). These SPNs were classified by their distinct responses to activation of the peripheral chemoreflex, diving response and arterial baroreflex, allowing the discrimination of muscle vasoconstrictor-like (MVC_{like}, 39%) from cutaneous vasoconstrictor-like (CVC_{like}, 28%) SPNs. The MVC_{like} SPNs have higher baseline firing frequencies (2.52 ± 0.33 Hz *vs.* CVC_{like} 1.34 ± 0.17 Hz, $P = 0.007$). The CVC_{like} have longer after-hyperpolarisations (314 ± 36 ms *vs.* MVC_{like} 191 ± 13 ms, $P < 0.001$) and lower input resistance (346 ± 49 MΩ *vs.* MVC_{like} 496 ± 41 MΩ, $P < 0.05$). MVC_{like} firing was respiratory-modulated with peak discharge in the late inspiratory/early expiratory phase and this activity was generated by both a tonic and respiratory-modulated barrage of synaptic events that were blocked by intrathecal kynurenate. In contrast, the activity of CVC_{like} SPNs was underpinned by rhythmical membrane potential

oscillations suggestive of gap junctional coupling. Thus, we have related the intrinsic electro-physiological properties of two classes of SPNs *in situ* to their roles in cardiorespiratory reflex integration and have shown that they deploy different cellular mechanisms that are likely to influence how they integrate and shape the distinctive sympathetic outputs.

Abbreviations   AHP, after-hyperpolarisation; CVC_{like}, cutaneous vasoconstrictor-like SPN; early-PI, early post-inspiratory; ECG, electrocardiogram; EPSC, excitatory postsynaptic current; EPSP, excitatory postsynaptic potential; late-I, late inspiration; MVC_{like}, muscle vasoconstrictor-like SPN; P, postnatal day; RVLM, rostral ventrolateral medulla; SPN, sympathetic preganglionic neurone; WHBP, working heart–brainstem preparation.

Introduction

The sympathetic preganglionic neurone (SPN) is one of the three main classes of CNS output cells (alongside the somatic motor neurone and the parasympathetic preganglionic neurone) and is responsible for integrating and generating the neural code to almost every tissue and organ in the body (Janig, 2006). Compared to its cholinergic neighbour, the somatic motor neurone, less is known about how their cellular properties and synaptic drives interact *in vivo* to produce the specific patterns of sympathetic outflow (Adrian *et al.* 1932). Yet it is clear that there are distinct patterns of discharge in the sympathetic outflow that are tailored to the diverse characteristics of the target organ/tissue and that these originate from parallel, labelled lines of sympathetic neurones (Dampney & McAllen, 1988; Morrison, 2001). Importantly, this sympathetic patterning is altered in disease conditions – such as hypertension, heart failure and diabetes – and this dysrhythmia is believed to be a substantial component of the pathology (reviewed by Robertson *et al.* 2012).

SPNs gatekeep the output from the CNS to the periphery and as such their intrinsic and network properties are proposed to be important in determining the patterning of activity reaching the end organs (such as blood vessels, secretory glands or brown fat) (Coote, 1988; Polosa *et al.* 1988). These integrative properties may enable SPNs to generate an output code that is tailored for the peripheral target tissues, which respond relatively slowly to incoming neural signals. Furthermore, this diversity of sympathetic target organs makes it likely that each outflow will have its own characteristic cellular and network tuning and coding properties.

From *in vitro* spinal cord slice recording studies it is apparent, across a range of species, that SPNs have some characteristic intrinsic properties that are likely to be important in the integration of the descending and segmental synaptic drives, such as a powerful transient rectification (Yoshimura *et al.* 1987*b*; Pickering *et al.* 1991; Sah & McLachlan, 1995; Zimmerman & Hochman, 2010; Whyment *et al.* 2011), slow and fast after-hyperpolarisations (AHPs; Yoshimura *et al.* 1986*a*, 1987*b*; Spanswick & Logan, 1990*b*; Sah & McLachlan, 1995), a T-type low threshold calcium conductance (Yoshimura *et al.* 1987*a*; Sah & McLachlan, 1995; Wilson *et al.* 2002) and the ability to generate bursting discharge (Yoshimura *et al.* 1987*a*; Spanswick & Logan, 1990*a*; Logan *et al.* 1996). There is also evidence that these properties are not uniformly distributed and several authors have attempted to subdivide the SPNs on the basis of these properties (Spanswick & Logan, 1990*b*; Pickering *et al.* 1991; Zimmerman & Hochman, 2010) but it has not been possible to identify these SPN characteristics as being associated with a particular end organ function.

This has left the question outstanding as to whether these differences in intrinsic properties are linked to the integrative role of the SPNs in cardiorespiratory reflexes *in vivo*. One study attempted to find differences in the intrinsic properties of SPNs innervating adrenergic or noradrenergic adrenal chromaffin cells using retrograde labelling from the adrenal medulla, anticipating (based on *in vivo* characterisation (Morrison & Cao, 2000)) that this would identify two groups; but the subsequent slice recordings identified an apparently homogenous population (Wilson *et al.* 2002). This *in vitro* approach of retrograde labelling from the target tissues is hampered in the sympathetic nervous system by the intervening ganglion synapse for all but the adrenal glands and, as yet, trans-synaptic techniques (Strack *et al.* 1989) have not been used for cellular recording studies.

An alternative strategy for identification of SPNs *in vivo* is on the basis of their response profile to activation of cardiorespiratory reflex afferents such as the arterial baroreflex, peripheral chemoreflex and naso-trigeminal afferents (diving response). This approach has been extensively employed to examine the unit responses of both pre- and postganglionic sympathetic units recorded in nerve trunks from cats and rats (Boczek-Funcke *et al.* 1992; reviewed by Janig, 2006). These studies provide a clear basis for the dissection of classes of sympathetic neurone into, for example, muscle vasoconstrictor-type

(MVC) or cutaneous vasoconstrictor-type (CVC) but these extracellular recording methods cannot resolve the cellular integrative processing at the level of the SPN that shape the final sympathetic output from the CNS. This is of particular interest in the case of the MVC class as alterations in the activity of this population of SPNs is implicated as being important for the generation of hypertension in animal models (Guyenet, 2006; Zoccal *et al.* 2008; Simms *et al.* 2009, 2010; McBryde *et al.* 2013) and in humans (Malpas, 2010; Esler, 2011; Fisher & Paton, 2012). However, the precise mechanisms of dysregulation of their excitability are still the subject of active debate.

Several notable studies have used intracellular recording to examine the properties of SPNs *in vivo* in the cat (Fernandez de Molina *et al.* 1965; Coote & Westbury, 1979; McLachlan & Hirst, 1980; Dembowsky *et al.* 1986). The most detailed of these showed similar intrinsic electrophysiology to that seen *in vitro* (Dembowsky *et al.* 1986) and further suggested that there were three different groups of SPNs on the basis of differences in their resting membrane potential and their AHP/after-depolarisation following action potential discharge. However, they were unable to show how the distinct properties of these groups of SPNs are linked to a particular functional role because of the inability to antidromically activate the neurones from their target tissue (because of the interposed ganglion) and of the difficulty of maintaining recordings while activating cardiorespiratory reflexes *in vivo* (see McLachlan & Hirst, 1980). Similarly the use of a medullary–spinal cord *in vitro* preparation, although allowing the study of descending synaptic drives to SPNs, did not allow the classification of the recorded neurones because of lost cardiorespiratory afferent connectivity (Deuchars *et al.* 1995).

To address this issue, we have used the working heart–brainstem preparation of neonatal rats to make whole cell patch clamp recordings from SPNs. We hypothesised in advance that we should be able to discriminate MVC_{like} and CVC_{like} SPNs on the basis of their dichotomous characteristic responses to chemoreflex and diving response activation. Hence we aimed to characterise the intrinsic properties of these classes of SPNs with reference to their role in cardiorespiratory integration.

Methods

Working heart–brainstem preparation

All experiments conformed strictly to the UK Home Office guidelines regarding the ethical use of animals and were approved by our institutional ethical review committee. The working heart–brainstem preparation (WHBP) was set up using previously described methods (Paton, 1996). In brief, male Wistar rats ($n = 59$, postnatal days 5–16) were deeply anaesthetised with halothane, until loss of withdrawal to paw pinch,

before the following surgical procedures: the rat was bisected sub-diaphragmatically, exsanguinated, cooled in carbogenated Ringer solution at 5–10°C, and suction decerebrated pre-collicularly following which the halothane anaesthesia was discontinued. The preparation was kept cold while the phrenic nerve, sympathetic chain and descending aorta were dissected free and a bilateral pneumonectomy was performed.

The preparation was positioned prone while still cold and access to the spinal cord was obtained via a laminectomy up to the level of C7. The dura was incised and the dorsal pia mater was removed locally at the level of T3. A single cut was made in the spinal cord using a custom built piezoslicer (designed by Dr J. Smith, NINDS-NIH, Bethesda, MD, USA (Smith *et al.* 2007)). This employed a piezoelectric bending actuator (Piezo Systems, Woburn, MA, USA) to oscillate a microblade (FST 10035-05) at 120 Hz with an amplitude of ∼0.5 mm maintaining the vibrating blade inside the walls of the trough of the spinal canal. This produced the 'slice *in situ*' preparation with a 45 deg bevel on the cut end of the cord starting at the dorsal surface and sloping caudad (Fig. 1). The spinal cord distal to the cut was freed of its tethering nerve roots and removed from the vertebral canal to give direct visual access to the lateral horn of the remaining rostral spinal cord at the level of T3 for recordings.

The time taken from the start of surgery to establishing artificial perfusion was typically between 20 and 25 min but the interval could be as long as 1 h without perfusion (to allow a more complex surgical preparation, e.g. aortic depressor nerve isolation – see below), with the preparation still cold, without detriment once perfusion was recommenced.

After transfer to the recording chamber a double lumen cannula was inserted into the descending aorta for retrograde perfusion with carbogen-gassed, modified Ringer solution (see below for composition) containing Ficoll-70 (1.25%; Sigma, St Louis, MO, USA) at 30°C. The perfusate was pumped from a reservoir flask, via a heat exchanger, through two bubble traps and a particle filter (25 μm screen, Millipore, Billerica, MA, USA) before passing via the cannula to the preparation. It was then recycled from the preparation chamber back to the reservoir and re-gassed. Flow was generated with a peristaltic pump (Watson-Marlow 505D, Falmouth, UK) with a maintained volume in the circuit of ∼200 ml. The perfusion pressure was monitored via the second lumen of the cannula.

The heart resumed beating almost immediately as the perfusate flow was gradually increased from ∼5 ml min^{-1} to a typical basal flow of 11–13 ml min^{-1}. As the preparation warmed up rhythmic respiratory muscle contractions were seen after 1–3 min, typically when the mean perfusion pressure reached 30–40 mmHg, signalling the return of brainstem function. At this point muscle relaxant

was added to the perfusion solution (vecuronium 200 μg; Norcuron, Organon, Cambridge, UK). The preparation was held in ear bars and positioned prone to allow access to the cut surface of the spinal cord. The lateral processes of the thoracic vertebrae were clamped to improve stability for recording.

Phrenic nerve recording

A glass suction electrode (tip diameter 200–300 μm) held in a micromanipulator was used to record from the phrenic nerve. These electrodes were pulled from borosilicate glass (GC150-F10, Harvard Apparatus, Edenbridge, UK) and broken back to the appropriate diameter to give a tight seal. To further improve the signal/noise ratio and reduce electrocardiogram (ECG) artefacts, these electrodes were of bipolar construction with the reference Teflon-coated silver wire electrode glued to the outside of the glass capillary such that its free end (bared of insulator) could be placed in close apposition to the nerve.

Signals were AC amplified and band pass filtered (80 Hz to 3 kHz). Rhythmic, ramping phrenic nerve activity, indicative of eupnoea, gave a continuous physiological index of preparation viability. During the initial phase of each experiment the preparation was fine-tuned to obtain a strong eupnoeic pattern of phrenic nerve activity and the presence of robust chemoreflex and baroreflex responses. This period of tuning aimed to produce a perfusion pressure of 30–40 mmHg by adjusting flow rate and/or the addition of vasopressin (Sigma) to the reservoir (200–400 pM). Once established in eupnoea, the preparation often required little further adjustment during the remainder of the experiment (typically 3–6 h). Additional silver electrode wires were employed to record ECG and a window discriminator was used to trigger from R-waves to derive instantaneous heart rate.

Whole cell recordings from SPNs

After optimisation of the incident illumination the outline of the lateral horn was clearly visible under a binocular microscope (Leica MZ-6) on the cut face of the cord (Fig. 1), allowing the recording patch electrode to be directed into the intermediolateral cell column containing the nests of SPNs. Blind, whole cell recordings were made from lateral horn neurones at depths of 50–500 μm below the cut surface. Electrodes were pulled from borosilicate capillaries (GC150-TF10, Harvard Apparatus, Holliston, MA, USA) to have a resistance of 5–10 MΩ when filled with pipette solution (see below). The pipette was advanced through the tissue with 30–100 mmHg positive pressure to keep the tip clear. Once at the desired depth, the pressure was reduced to <10 mmHg to search for cells, which was released on detection of a cell, followed by

application of gentle suction to form a GΩ seal. Further negative pressure was applied to rupture the seal allowing stable recordings to be made from neurones for periods of over 1 h with access resistances of 20–50 MΩ. In some experiments the broad spectrum excitatory amino acid antagonist kynurenate (30–50 mM, Tocris, Bristol, UK) was applied by local superfusion over the cut surface of the spinal cord to block spinal excitatory synaptic transmission.

Current clamp and any subsequent voltage clamp recordings were made using a discontinuous clamp amplifier (SEC-05LX-BF, NPI electronic, Tamm, Germany) with switching frequencies between 10 and 15 kHz and a 25% duty cycle after optimisation of capacitance compensation. The gain was maximally increased to just below the point of clamp instability (typically around 1000×) as assessed from continuous monitoring of the electrode potential output. Cell recordings were low pass filtered at 2 kHz and the signal passed through a Humbug (Digitimer, Welwyn Garden City, UK) to remove mains interference. Data were sampled at 5 kHz using a power1401 analog/digital converter (CED, Cambridge, UK).

Lateral horn neurones were antidromically identified as being SPNs by activation following stimulation (0.3–1 ms, 5–20 V, 0.2–20 Hz) of the ventral root exit zone of the spinal cord with a concentric bipolar electrode (Fig. 1; SNE100, Rhodes Medical Instruments, Carpinteria, CA, USA). Cancellations were sought by depolarising the cell to fire spontaneous action potentials while applying ventral root stimuli. A total of 46/62 (74%) of the SPNs tested were identified antidromically. The remaining cells were identified as putative SPNs on the basis of characteristic electrophysiology, *post hoc* anatomical reconstruction and by their responses to functional reflex activation (see below).

Cardiorespiratory reflex activation

In each neonatal WHBP the afferent stimulus was titrated at the start of the experiment to reproducibly evoke the expected physiological responses.

Peripheral chemoreceptors were stimulated using intra-arterial injection of sodium cyanide (50–100 μl of 0.03%) as a bolus into the perfusion line. The chemoreflex responses were dose-dependent and the doses used produced sub-maximal bradycardia (1–2 Hz) and hyperpnoea.

The diving response was evoked by application of cold Ringer solution (∼10°C, 50–200 μl) to the snout that triggered a characteristic apnoea (lasting for > 2× basal respiratory cycle period) and transient bradycardia.

Attempts to activate the arterial baroreflex while maintaining a stable recording proved challenging as both

ramp increases in pressure (produced by increasing the flow from the peristaltic pump) and also intra-arterial boluses of phenylephrine (5–10 μg, $n = 27$ cells) caused most cells to be lost during or immediately after the stimulus. Therefore in some preparations ($n = 23$) the left aortic depressor nerve (ADN) was exposed and isolated in the cervical region, cut and the proximal end aspirated into a fine glass bipolar suction stimulating pipette. The nerve was activated with current pulses (0.1–1 ms, 5–600 μA, 30 Hz, 5 s) titrated at the start of the preparation to evoke a bradycardia of ~1 Hz. This approach allowed the effect of baroafferent activation to be tested in 34 SPNs.

SPN recording protocol

Following seal rupture the initial recordings were made in current clamp mode and the cell was allowed to stabilise before:

  i. baseline current clamp recording of firing activity (~1 min)
 ii. diving response (cold Ringer solution to snout) and peripheral chemoreflex activations (NaCN I.A.)
iii. aortic depressor nerve activation (if isolated for stimulation)
 iv. voltage responses to injection of current pulses
  v. antidromic identification test
 vi. voltage clamp to resolve synaptic events underlying the basal firing and the response to cardiorespiratory afferent activation
vii. spinal application of kynurenate (and wash) to examine the pharmacological sensitivity of the ongoing synaptic activity

This protocol took ~ 30 min to complete, allowing sufficient time for the preparation/cell to recover to baseline after each test. As such there was a dropout rate during the cell recordings and the tests were applied in priority sequence and those least likely to risk losing the recording.

Post hoc histological processing

Spinal tissue was removed after recording in a number of preparations ($n = 24$). In most cases several recordings would have been made from the preparation so although it was possible to confirm that SPNs were recorded from a particular preparation it was often not possible to unambiguously attribute that morphology *post hoc* to a particular cell recording. The tissue was fixed by immersion in 10% formaldehyde in PBS. After overnight cryoprotection in 30% sucrose the spinal cord was cut into 60–80 μm sections on a freezing microtome and mounted for fluorescence microscopic examination.

Data recording and analysis

Perfusion pressure, ECG and phrenic nerve activity were recorded using custom built AC amplifiers and transducers (designed and built by J. Croker, University of Bristol) and collected via an analog/digital interface (power1401, CED) to a computer running Spike2 software (CED). Custom scripts were used for data acquisition and analysis in Spike2.

All membrane potentials were corrected for a junction potential of 13 mV. SPNs with resting membrane potentials greater than −40 mV and whose action potentials overshot zero were considered to be healthy and were included for the analysis of membrane properties. Spike parameters were measured from spontaneous action potentials in a large majority of cases, and in the case of silent cells ($n = 7$) the cell was depolarised by current injection to the point where action potential discharge began to occur. The threshold for spike discharge was taken arbitrarily as the point at which the rate of rise of membrane potential exceeded 7.5 V s^{-1}. Subsequent spike parameters were measured with reference to this threshold point. Spike amplitude was measured above threshold and duration was calculated at one-third spike amplitude. The duration of the AHP was calculated from where spike repolarisation crossed threshold to the point of return to resting potential. AHP amplitude was measured from spike threshold to the trough. Input resistance and time constant were estimated by measuring the voltage deflection (amplitude 5–10 mV) in response to small hyperpolarising current pulses.

Statistical analysis

Data are expressed as mean ± standard error or median [interquartile range]; '*n*' refers to the number of cells. Two tailed *t* tests or analysis of variance (ANOVA) was used to establish statistical significance (Prism 5, Graphpad Software, San Diego, CA USA). Statistical significance was defined as $P < 0.05$.

Drugs and solutions

The composition of the modified Ringer solution used as perfusate was (mM): NaCl, 125; NaHCO$_3$, 24; KCl, 3; CaCl$_2$, 2.5; MgSO$_4$, 1.25; KH$_2$PO$_4$, 1.25; dextrose, 10; pH 7.35–7.4 after carbogenation. The patch solution contained (mM): potassium gluconate, 130; KCl, 10; NaCl, 10; MgCl$_2$, 2; Hepes, 10; NaATP, 2; NaGTP, 0.2 (pH 7.4 and osmolarity 300 mosmol l^{-1}). Lucifer yellow was added to the pipette solution (1 mg ml^{-1}) in some cases to enable *post hoc* morphological identification. All chemicals were from Sigma (UK).
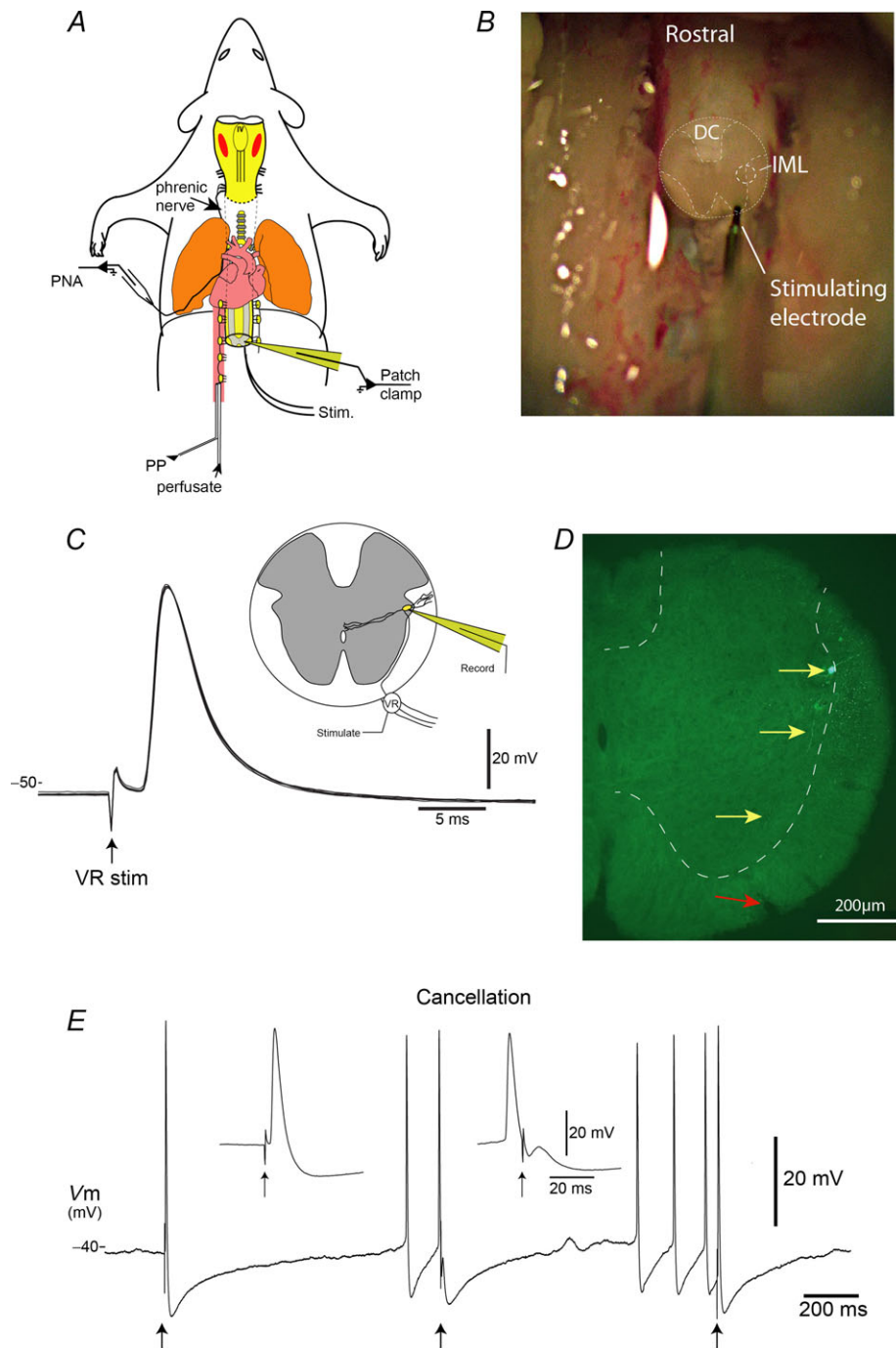
Figure 1. Accessing SPNs *in situ* in the working heart brainstem preparation
A, schematic WHBP of a decerebrate, artificially perfused preparation of rat (aged 5–16 days). The preparation is maintained at 32°C and recordings of phrenic nerve, perfusion pressure and heart rate are made to ensure that a eupnoeic pattern of discharge and cardiorespiratory reflex function are preserved indicating brainstem viability. *B*, the spinal cord is exposed through a dorsal laminectomy from T1 to T7 and an oblique cut made from dorsal to ventral through the cord at T3–4 level using the piezo-slice with the preparation still cold. The lateral horn is visible (IML) and patch pipettes were directed using a binocular stereozoom microscope to make blind whole cell recordings. SPNs were antidromically identified by placing a concentric bipolar stimulating electrode on the ventral root/ventral root exit zone. DC, dorsal columns. *C*, antidromic activation of an SPN from the ventral root (five overlaid consecutive traces). The same SPN is shown in *E* when it is depolarised to produce orthodromic action potentials demonstrating cancellations, which was taken as confirmation of antidromic identification. *D*, *post hoc* histological recovery of a Lucifer Yellow-filled SPN in the lateral horn with its axon extending to the ventral root (60 μm section).

Table 1. Electrophysiological properties of SPNs

	Mean ± SEM	*n*
Resting potential (mV)	−51.8 ± 0.5	98
Input resistance (MΩ)	416 ± 26	83
Time constant (ms)	34.5 ± 2.3	77
Firing frequency (Hz)	2.0 ± 0.2	98
Spike threshold (mV)	−42.1 ± 0.4	98
Spike amplitude (mV)	47.9 ± 0.8	98
Spike duration (ms)	3.65 ± 0.10	98
AHP amplitude (mV)	−18.1 ± 0.4	98
AHP duration (ms)	231 ± 14	98

Results

Stable whole-cell patch clamp recordings were made from 253 neurones in the lateral horn of the T3–4 segments of neonatal rat spinal cord (from 59 preparations, aged 10 [8–12 interquartile range] days postnatal). These recordings included a variety of cell types besides SPNs, including deep dorsal horn neurones and somatic motoneurones. Of these cells, 46 were antidromically identified as being SPNs on the basis of action potential discharge evoked from the ventral root exit zone with cancellations ($n = 46/62$ (74%) tested (Fig. 1*C* and *E*)). A further 52 were identified as being SPNs on the basis of their characteristic electrophysiological properties (see Table 1) with long duration action potentials (Fig. 1*C*), large prolonged AHP (Figs 1*E* and 2*A*), limited maximal spike discharge frequency (Fig. 2*A*), and the presence of transient and anomalous rectification (Fig. 2*A*), as has previously been documented *in vivo* (Dembowsky *et al.* 1986) and in slice preparations *in vitro* (Yoshimura *et al.* 1986*b*, 1987*b*; Pickering *et al.* 1991; Wilson *et al.* 2002). This identification was complemented by *post hoc* anatomical scrutiny (from 28 WHBPs) revealing labelled cells showing the typical somato-dendritic morphology of SPNs with an axon passing out of the ventral horn (Fig. 1*D*) and extended by the characteristic patterns of responses to cardiorespiratory reflex activation (see below).

Intrinsic electrophysiological properties of SPNs *in situ*

The SPNs had resting potentials of −51.8 ± 0.5 mV ($n = 98$) and the majority fired action potentials under baseline conditions (95%, $n = 93$) at an average rate of 2.0 ± 0.2 Hz. These action potentials were discharged from a threshold for initiation of −42.1 ± 0.4 mV. The SPNs exhibited ongoing excitatory postsynaptic potentials (EPSPs) which could be seen to summate to generate spike discharge (Fig. 2*B*). Their input resistance was 416 ± 26 MΩ ($n = 83$) and the membrane time constant was 34.5 ± 2.3 ms ($n = 77$).

The action potentials had an amplitude of 47.9 ± 0.8 mV above threshold and duration at one-third height of 3.65 ± 0.1 ms. The spike was followed by an AHP of amplitude −18.1 ± 0.4 mV lasting for 231 ± 14 ms. In response to hyperpolarising current pulses that took the membrane potential more negative than −80 mV, an anomalous rectification was seen in 80% of SPNs (41/51, Fig. 2*Aa* and *Ac*) followed at the offset of the pulse by a delayed return to resting potential indicative of the presence of a slow transient rectification (73%, 37/51, Fig. 2*Aa*). The injection of depolarising current pulses incrementally increased their firing rate up to a maximum of 10.6 ± 0.7 Hz ($n = 49$, 30 pA current pulse, Fig. 2*Ab*). After a train of action potentials, many of the SPNs exhibited a slow AHP that produced a prolonged hyperpolarisation (lasting several seconds) and reduction in action potential discharge (Fig. 2*Ab*).

Comparison of the electrophysiological properties of the antidromically identified SPNs ($n = 46$) and those putative SPNs that either failed on antidromic testing ($n = 16$) or were untested ($n = 36$) showed that they were indistinguishable for all measured parameters (Table 2), suggesting that they were sampled from the same population of SPNs.

Cardiorespiratory reflex response classification of SPNs

SPNs were classified in line with previously described criteria (Janig, 2006) on the basis of their responses to activation of the peripheral chemoreflex, diving response and arterial baroreflex afferent activation. The autonomic responses of the WHBP to activation of these cardiorespiratory afferents have previously been characterised (Paton, 1996; Dutschmann & Paton, 2002; Pickering *et al.* 2002; Braga *et al.* 2007; Simms *et al.* 2007). An adequate afferent stimulus was defined for each neonatal WHBP to reproducibly evoke the characteristic physiological response (see Methods and Fig. 3).

Each SPN was classified as being either excited (firing frequency increased/membrane potential depolarised), inhibited (firing frequency decreased or hyperpolarised) or unaffected by afferent stimulation (see Table 3). In equivocal cases a larger stimulus was re-applied to attempt to elicit a response.

Peripheral chemoreflex activation

Activation of the peripheral chemoreflex with intra-arterial NaCN (15–30 μg) produced the expected increase in phrenic discharge and bradycardia in all preparations but bisected the population of SPNs into those that were excited ($n = 44$, 45%, Fig. 3*Ab*) and a group that was inhibited ($n = 46$, 47%, Fig. 3*Bb*). The
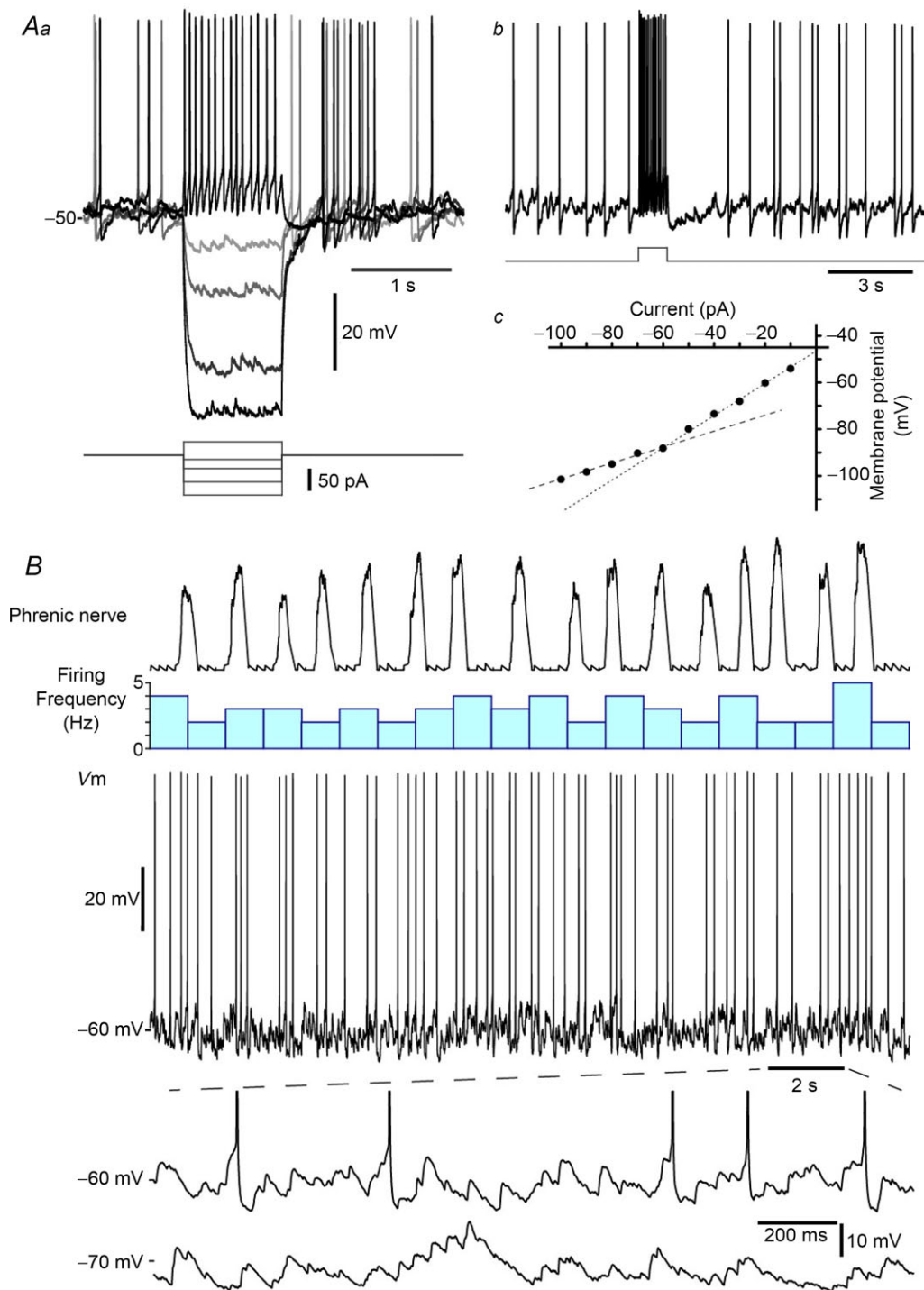
Figure 2. Typical SPN electrophysiology and spontaneous firing
A, current clamp recording of an SPN firing spontaneously at rest. This firing was inhibited by the injection of a family of hyperpolarising current pulses (1 s) and the cell showed both anomalous inward rectification at potentials more negative than −80 mV (shown on the *I–V* plot in *Ac*) and a transient rectification following the offset of the larger pulses. The end of this delayed return to rest was often marked by a period of rebound excitation and action potential discharge. Depolarisation increased action potential discharge and was followed at the offset of the pulse by a slow AHP with reduced firing for a period of several seconds (shown on a slower timescale in *Ab*). *B*, spontaneous pattern of discharge of another SPN (spike rate histogram shown alongside ongoing phrenic activity). This activity was driven by incoming EPSPs, as shown expanded beneath. The injection of a hyperpolarising DC current allowed the summation of these excitatory events to be clearly seen.

Table 2. Comparison of properties of antidromically identified and putative SPNs

	SPNs		Putative SPNs			
	Antidromic +ve	*n*	Antidromic –ve	*n*	Not tested	*n*
Resting potential (mV)	−52.3 ± 0.8	46	−50.8 ± 1.2	16	−51.7 ± 0.7	36
Input resistance (MΩ)	398 ± 32	44	415 ± 65	16	454 ± 55	23
Time constant (ms)	39.5 ± 3.4	42	28.3 ± 5.2	13	28.6 ± 3.4	22
Firing frequency (Hz)	1.82 ± 0.27	46	2.52 ± 0.5	16	2.08 ± 0.33	36
Spike threshold (mV)	−42.0 ± 0.7	46	−41.0 ± 1.2	16	−42.6 ± 0.6	36
Spike amplitude (mV)	49.7 ± 1.3	46	48.2 ± 2.4	16	45.5 ± 1.1	36
Spike duration (ms)	3.69 ± 0.12	46	3.73 ± 0.30	16	3.57 ± 0.18	36
AHP amplitude (mV)	−18.6 ± 0.5	46	−18.0 ± 0.7	16	−17.4 ± 0.65	36
AHP duration (ms)	235 ± 21	46	194 ± 24	16	242 ± 23.9	36

Antidromic testing showing orthodromic cancellations identified 46 SPNs (20 MVC$_{like}$ (52%), 14 CVC$_{like}$ (52%), 7 chemo inhibited/diving excited (44%), 3 chemo excited/diving inhibited (50%)). A further 52 were identified as putative on the basis of characteristic electrophysiology and pattern of responses to cardioreflex afferent activation. Of these, 16 failed on antidromic testing either because no collisions were evident (*n* = 7) or because there was no evoked spike (*n* = 9). No significant difference was found in any parameter between antidromically identified and putative SPN groups (antidromic –ve or untested, one-way ANOVA).

excitatory responses were characterised by an increase in spike firing frequency and a small depolarisation. This typically lasted for the duration of the bradycardia and increase in phrenic firing. In contrast the inhibitory responses were associated with a striking fall in firing frequency accompanied by a hyperpolarisation. Only two SPNs did not show any response to chemoreflex activation. Recordings from different SPNs showing either excitatory or inhibitory responses to chemoreflex activation could be seen in the same preparation (in a total of 12 WHBPs).

Diving response

Activation of the diving response by the application of cold saline to the snout excited a majority of SPNs (*n* = 55, 56%, Fig. 3*Aa*) with most of the remainder being inhibited (*n* = 34, 35%, Fig. 3*Ba*). The excitatory responses were characterised by an increase in spike firing frequency and a depolarisation. This typically lasted for the duration of the apnoea. In contrast, the inhibitory responses were associated with a reduction in firing frequency and accompanied by a hyperpolarisation. Again only two cells did not show any response to diving response activation. Different SPNs showing either excitatory or inhibitory responses to diving response activation were seen in neurones recorded in the same preparation (*n* = 9 WHBPs).

Arterial baroreflex

We analysed the response of 32 SPNs to electrical activation of the aortic depressor nerve; 19 of 32 (59%) SPNs showed clear inhibitory responses (Fig. 4) with the remaining 12 showing no response (no cells were excited by ADN stimulation). This inhibition was time locked to the nerve stimulation with a rapid onset (starting within

100 ms of the first stimulus) and a slower offset (firing resumed within 0.5 s of the last stimulus).

Identification of SPNs with muscle vasoconstrictor characteristics

The largest population of SPNs identified showed excitatory responses to activation of the peripheral chemoreflex and also during the diving response (*n* = 38/98 (39%); Fig. 3*A* shows typical responses) and were inhibited by baroafferent stimulation. These response characteristics have been reported previously for muscle vasoconstrictor-type sympathetic neurones and henceforth we refer to them as being MVC$_{like}$. Under basal conditions the MVC$_{like}$ SPNs exhibited ongoing action potential discharge with a respiratory modulated pattern (significantly increased firing in late inspiration (late-I) and the early post-inspiratory (early-PI) phase (see Fig. 5*A* and *C* baselines and the pooled data in Fig. 6*A*). This firing was driven by incoming bursts of EPSPs/excitatory postsynaptic currents (EPSCs) (see Fig. 7) and there was no evidence of spontaneous rhythmic oscillatory activity. The incoming excitatory potentials were blocked by the spinal superfusion of kynurenate (50 mM, *n* = 5, see Fig. 8). This respiratory-modulated, fluctuating excitatory synaptic drive was superimposed on a tonic 22.8 ± 8 pA (*n* = 4, SPNs voltage clamped at resting potential) inward current generated by summated EPSCs (Fig. 8) that was revealed by the kynurenate blockade. Using an event discrimination algorithm (Spike2) to identify the larger synaptic events (of magnitude >20 pA) we found that these were arriving at a frequency of 19.6 ± 7.1 Hz, which was significantly reduced in the presence of spinal kynurenate (1.6 ± 1.9 Hz, *P* < 0.05, *n* = 5), giving an indication of the magnitude of the ongoing excitatory amino acid-mediated synaptic barrage driving activity.
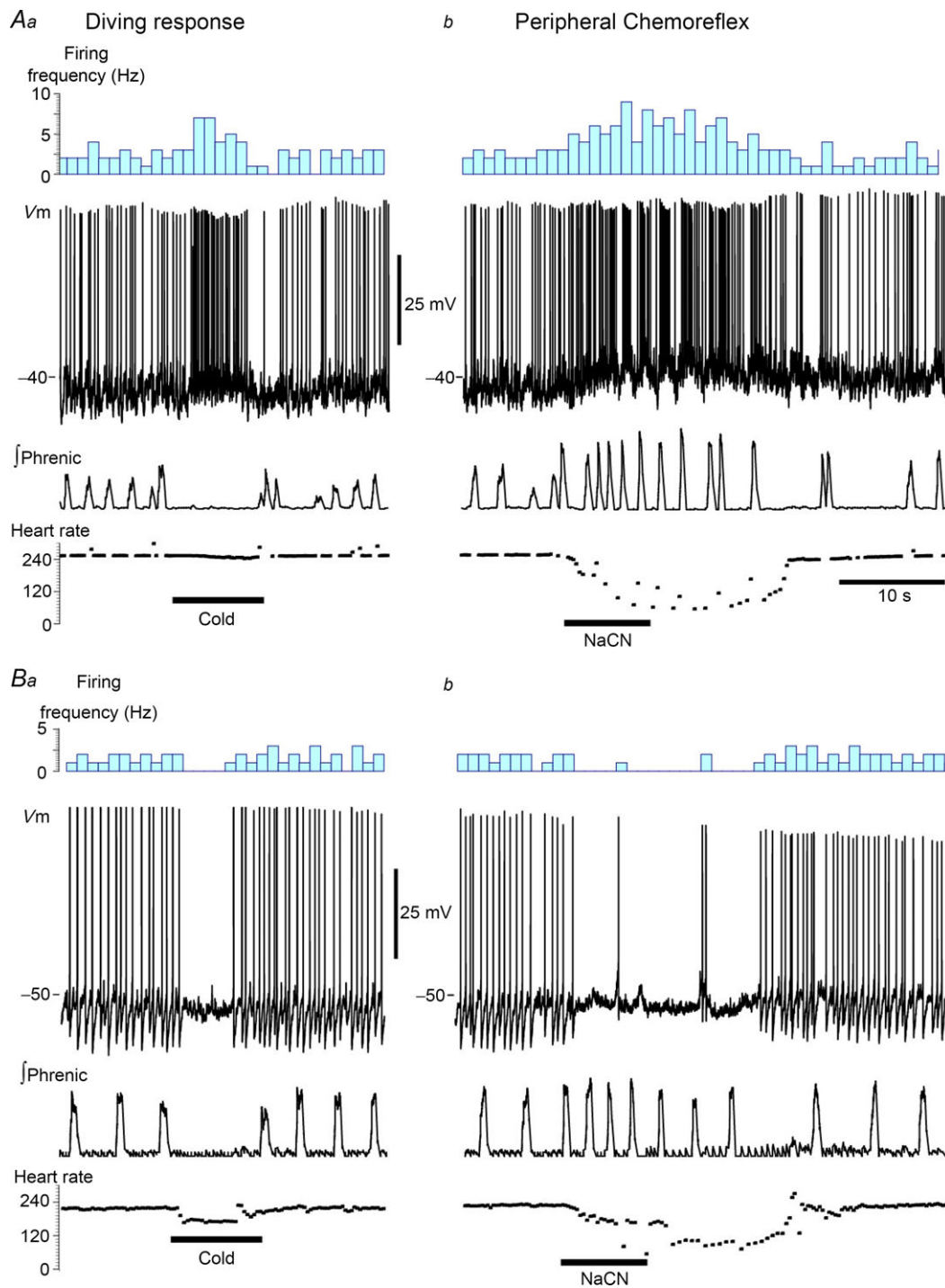
Figure 3. Identification of SPN subtypes by response to cardiorespiratory reflex activation
Responses of SPNs to activation of peripheral chemoreflex (NaCN 0.05 ml, 0.03%, I.A.) and diving reflex (cold Ringer solution to snout ~10°C, 50–200 μl). Activation of the diving response produced a transient apnoea and a reduction in heart rate whereas activation of the peripheral chemoreflex caused an increase in respiratory frequency and phrenic amplitude along with a marked bradycardia. *Aa,b*, an SPN showing excitatory responses to both reflexogenic stimuli. The excitation in both cases more than doubles the spontaneous rate of action potential discharge and only lasts for the period of the change in heart rate and respiratory pattern. In the case of the chemoreflex (*Ab*) response the degree of respiratory modulation of the firing activity is enhanced to produce a clear bursting pattern. *Ba,b*, a different SPN showing inhibition of firing and hyperpolarisation during both the diving response and activation of the peripheral chemoreflex. In both cases the onset of the effect is prompt, the duration of the inhibition does not outlast the period of bradycardia and the cell returns to its previous firing pattern.

Table 3. Matrix of responses of SPNs to stimulation

Peripheral chemoreflex		Excited (n = 55)	Inhibited (n = 34)	Nil (n = 2)	Not tested (n = 7)
	Not tested (n = 6)	0	0	0	6
	Nil (n = 2)	1	1	0	0
	Inhibited (n = 46)	16	27	2	1
	Excited (n = 44)	38	6	0	0
	Total (n = 98)	Excited (n = 55)	Inhibited (n = 34)	Nil (n = 2)	Not tested (n = 7)
	Diving response				

Peripheral chemoreceptors were stimulated using intra-arterial injection of sodium cyanide (50–100 μl of 0.03%) as a bolus into the perfusion line. The diving response was elicited by application of cold Ringer solution ($\sim$10°C, 50–200 μl) to the snout that triggered a characteristic apnoea and transient bradycardia that are characteristic for stimulation of nasotrigeminal afferents.

Chemoreflex activation increased the firing rate of MVC$_{like}$ SPNs (from 3.02 $\pm$ 0.61 to 4.95 $\pm$ 0.96 Hz, $P = 0.002$, $n = 11$) driven by a summating barrage of EPSPs that depolarised the membrane (from -47.5 ± 1.8 to -44.9 ± 1.6 mV, $P = 0.0001$, $n = 11$). This exaggerated the respiratory modulation of spike discharge and produced a shift in the phase relationship (demonstrated by respiratory-triggered phase histogram analysis, $n = 4$) with the increase in spike discharge concentrated into the late-I/early-PI period (see Fig. 5).

Activation of the diving response produced an apnoea and a transient, robust increase in the firing of the MVC$_{like}$ SPNs (from 3.27 $\pm$ 0.71 to 7.5 $\pm$ 0.97 Hz, $P = 0.00002$, $n = 11$) driven by a barrage of EPSPs that summated to depolarise the membrane (-47.7 ± 1.7 to -45.2 ± 1.6 mV, $P = 0.00005$, $n = 11$, Fig. 3Aa). This also uncoupled the discharge of the SPNs from the respiratory cycle such that they now fired during the period of apnoea.

Activation of arterial baroreflex afferents triggered a powerful inhibition of MVC$_{like}$ SPNs (12/14 (86%) tested; Fig. 4 shows an example of baroafferent inhibition of MVC$_{like}$ SPNs). The ADN stimulus reduced heart rate by 1.1 ± 0.16 Hz and caused an inhibition of the spontaneous discharge of the SPNs by 2.0 ± 0.7 Hz ($n = 12$, reduced the firing rate by 43 ± 9%). This inhibition was tightly time-locked to the ADN stimulus train with a rapid onset/offset.

Identification of SPNs with a cutaneous vasoconstrictor response profile

In contrast, a second substantial population of SPNs ($n = 27/101$, 27%) were inhibited by peripheral chemoreflex activation and also inhibited during the diving response (Fig. 3B), a profile that has previously been associated with cutaneous vasoconstrictor sympathetic neurones and henceforth are referred to as being CVC$_{like}$. The firing pattern of these SPNs was distinct from that of the MVC$_{like}$ SPNs (Fig. 6C) and although this showed respiratory modulation, spike discharge was significantly lower in the late-I and early-PI phase than the expiratory phase (in counter-phase to the MVC$_{like}$, see Fig. 6B). The firing in CVC$_{like}$ SPNs was driven by underlying stereotyped membrane potential oscillations (14/15 tested, Fig. 9B and C) with a relatively sparse EPSP drive compared to the MVC$_{like}$ SPNs. These biphasic events were indistinguishable from those previously noted in a population of gap junction-coupled SPNs *in vitro* (Spanswick & Logan, 1990a; Logan *et al.* 1996; Nolan *et al.* 1999).

Peripheral chemoreflex activation reduced their firing rate (from 1.54 $\pm$ 0.24 to 0.41 $\pm$ 0.20 Hz, $P = 0.0002$, $n = 12$; Fig. 3Bb) driven by a hyperpolarisation of the membrane (from -50.2 ± 1.2 to -55.7 ± 1.5 mV, $P = 0.0001$, $n = 12$). This inhibition commenced promptly with the onset of the increased respiratory drive and bradycardia of the chemoreflex and did not outlast the end of the cardiorespiratory response.

Activation of the diving response produced an apnoea and a transient but marked inhibition of the firing of CVC$_{like}$ SPNs (from 1.75 $\pm$ 0.2 to 0.33 $\pm$ 0.13 Hz, $P = 0.00002$, $n = 12$) associated with a membrane hyper-polarisation (-50.8 ± 1.2 to -54.0 ± 2.0, $P = 0.0086$, $n = 12$; Fig. 3Ba). Stimulation of the aortic depressor nerve to activate arterial baroreflex afferents (producing a bradycardia of 1.0 ± 0.18 Hz) was either without effect (4/7) or only modestly reduced spike discharge (3/7 tested, only one of these SPNs was inhibited by > 30%).

## Comparison of the properties of MVC_like and CVC_like SPNs

These two categories of SPNs had many cellular properties in common (see Table 4) with similar resting membrane potentials, characteristic long duration action potentials, large AHPs and anomalous rectification. However, there were also some major differences in the intrinsic electrophysiological and network properties of these subtypes. The MVC_like SPNs compared to CVC_like have higher baseline firing frequencies (2.52 ± 0.33 *vs.* 1.34 ± 0.17 Hz,

$P < 0.01$). The CVC_like SPNs have longer AHPs (314 ± 36 *vs.* 191 ± 13 ms, $P < 0.001$) and a lower input resistance (346 ± 49 *vs.* 496 ± 41 MΩ, $P < 0.05$). Almost all of the MVC_like SPNs examined (90%, $n = 21$) showed both anomalous rectification, transient rectification and a slow AHP that followed a train of action potentials evoked by depolarising current pulses (Fig. 2Ab). In contrast, significantly fewer of the CVC_like SPNs showed anomalous rectification (56%, $n = 9/16$, $P < 0.05$), transient rectification (33%, $n = 6/18$, $P < 0.001$) or the slow
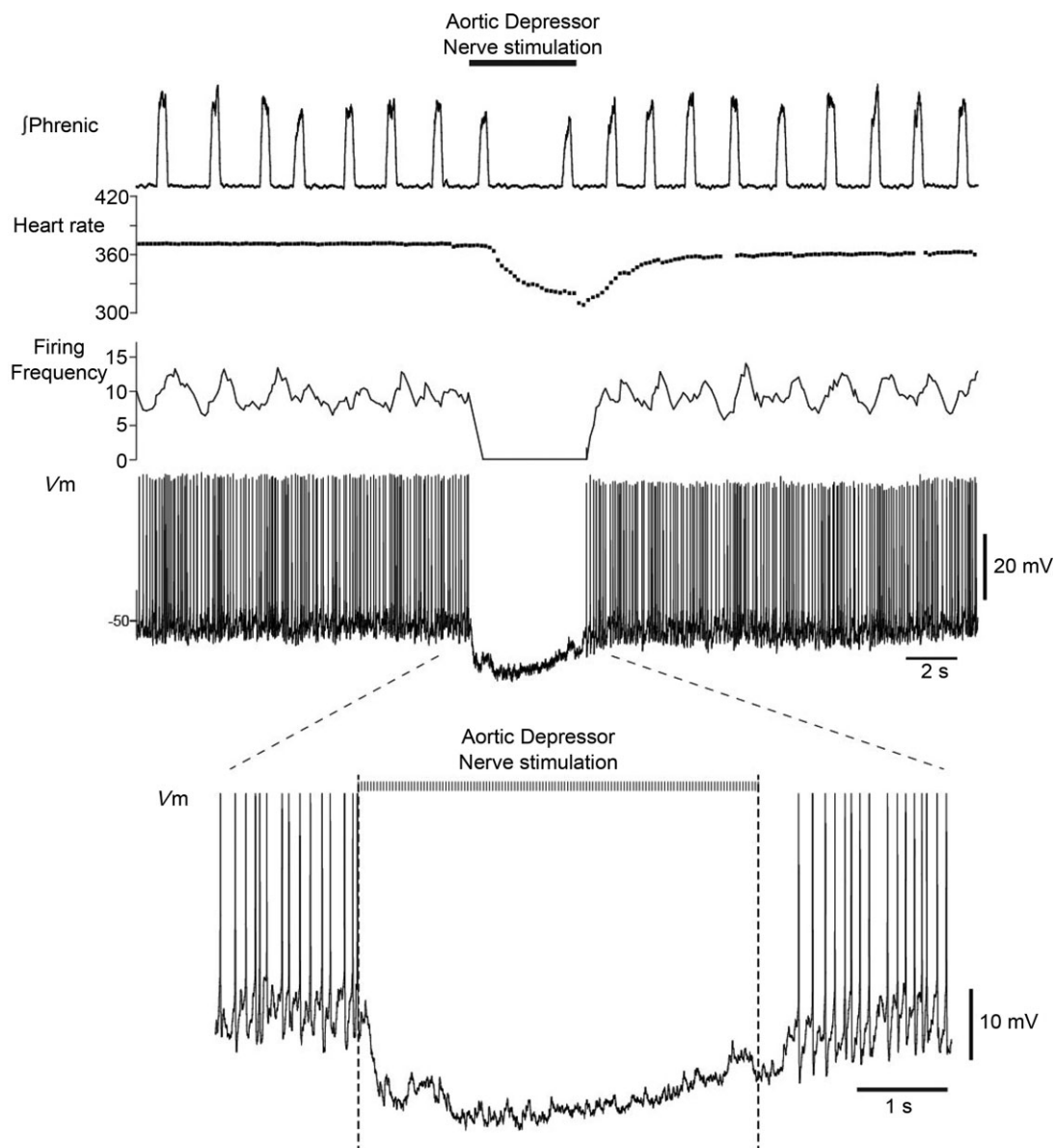
Figure 4. Inhibition of SPNs by arterial baroreceptor activation
Electrical stimulation of the aortic depressor nerve (30 Hz, 0.1 ms, 500 μA, 5 s) produced a marked bradycardia (60 b.p.m.) and a complete inhibition of the spontaneous activity of this SPN. This was accompanied by a hyperpolarisation of >10 mV. As can be seen from the expanded trace below, this baro-inhibition had a rapid onset after the start of stimulation (the hyperpolarisation commenced within 100 ms) and a slower but still prompt recovery after stimulation ceased.
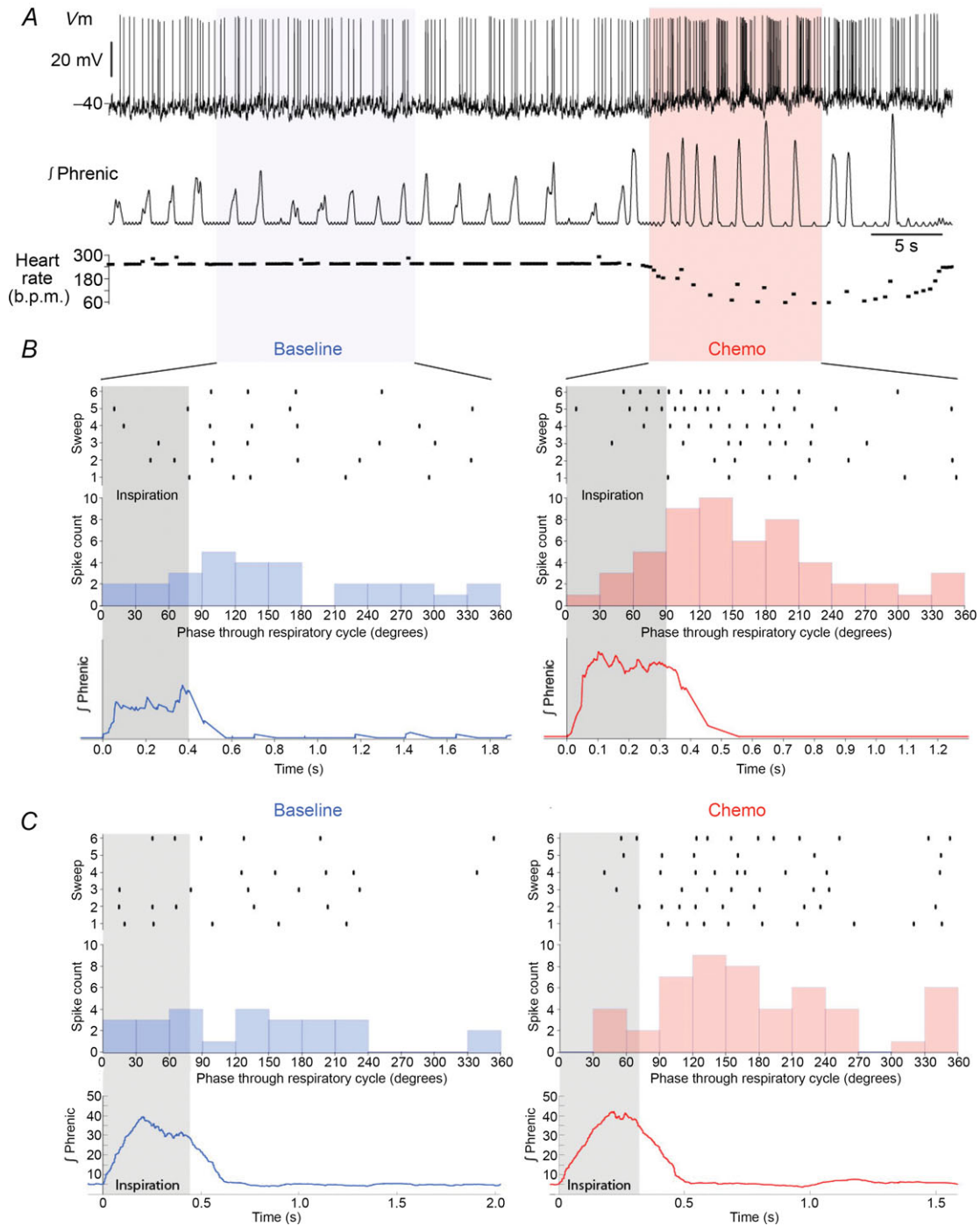
Figure 5. Peripheral chemoreflex activation enhances respiratory-sympathetic coupling of MVC$_{like}$ SPN discharge

A, action potential firing of an MVC$_{like}$ SPN (same as that shown in Fig. 3) before (left) and during activation of the peripheral chemoreflex with NaCN. Respiratory phase analysis (over six respiratory cycles, cumulative spike count) shows that under control conditions the SPN fires most commonly in the late-I and early-PI periods (average phrenic signal shown below). This is augmented by activation of the peripheral chemoreflex with the increase in firing activity contained within this period of the respiratory cycle. *B*, another MVC$_{like}$ SPN showing the respiratory phase analysis with preferential discharge in the inspiratory/post-inspiratory period under basal conditions. Activation of the peripheral chemoreflex again increased firing, with the majority of the excitation found in the post-I period. Note also that action potential discharge is now relatively inhibited in early inspiration. This analysis was conducted on four MVC$_{like}$ SPNs, all of which showed a similar pattern of early inspiratory inhibition and post-inspiratory excitation following NaCN application.

AHP (53%, 9/17, $P < 0.05$ all comparisons with MVC_{like} using Fisher's exact test, Fig. 9*A*). These cells also had distinct patterns of respiratory modulation with the peak firing in MVC_{like} SPNs during late-I/early-PI whereas this same period was the nadir in the firing of CVC_{like} SPNs (Fig. 6).

Other classes of SPNs

The next largest group of SPNs were inhibited by peripheral chemoreflex activation and were excited during the diving response ($n = 16/101$, 16%). Only one of six tested (17%) was inhibited by ADN stimulation. They showed spontaneous discharge at an average of 1.89 ± 0.67 Hz ($n = 15/16$) from a resting potential of -50 ± 1.0 mV

($n = 16$) without a consistent pattern of respiratory modulation but driven by incoming EPSPs.

A small group of SPNs were excited by peripheral chemoreflex activation and inhibited during the diving response (6/101, 6%). They showed heterogeneous patterns of activity with only two showing clear respiratory modulation of their basal firing. There were too few cells in this heterogenous group for meaningful comparisons of their parameters with the other cell types. None of the cells had their response to arterial baroafferent stimulation examined.

Under our experimental conditions only six cells were recorded that were essentially silent under baseline conditions (<0.02 Hz). Each showed ongoing sub-threshold synaptic activity and all demonstrated
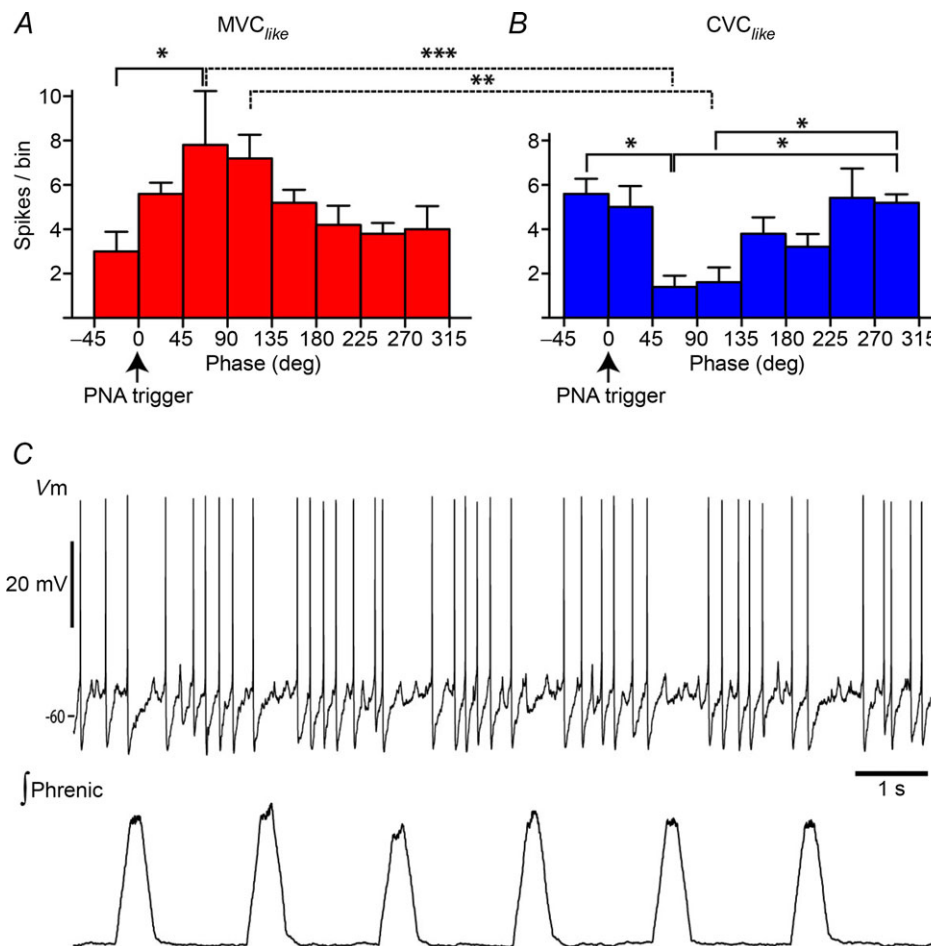
Figure 6. Comparison of spontaneous patterns of MVC$_{like}$ and CVC$_{like}$ respiratory coupling
Respiratory phase discharge bar charts for (*A*) MVC$_{like}$- and (*B*) CVC$_{like}$ SPN averaged from five cells of each class and across 10 respiratory cycles. The MVC$_{like}$ SPNs show a distinctive pattern of modulation with a peak of activity in the late-I/early-PI phase (45–90 deg) which is significantly larger than the level of activity seen in the late E phase (-45–0 deg, $P < 0.05$, one-way ANOVA with Bonferroni post tests). In contrast ,the CVC$_{like}$ SPNs showed an inhibition of their activity over the same period with a significant nadir in the same late-I/early-PI phase. These distinctions in respiratory modulation of firing pattern are also significantly different across the two groups (dotted brackets, **$P < 0.01$, ***$P < 0.001$, two-way ANOVA with Bonferroni post tests). *C*, spontaneous activity of a CVC$_{like}$ SPN with the phrenic activity below showing the characteristic pattern of pauses in firing with inspiration followed by discharge in expiration.

clear responses to cardiorespiratory afferent activation, allowing them to be identified as belonging to the following classes of SPN: MVC_{like} ($n = 4$), CVC_{like} ($n = 1$) and one cell in the chemoreflex inhibited/diving response excited class.

Discussion

We have been able to relate the distinct intrinsic electrophysiological properties of SPNs to their roles in cardiorespiratory reflex integration. This has allowed us to examine the synaptic input and network interactions that underpin the generation and flux of sympathetic tone to the periphery and has emphasised the importance of the intrinsic properties of SPNs in the integration of these complex drives. We have contrasted these cellular and network properties of the MVC_{like} with CVC_{like} SPNs and have extended our understanding of the contribution of this specialisation to the generation of the distinctive patterns of sympathetic outflow.

There has previously been a lack of experimental data linking the intrinsic properties of SPNs to their roles *in vivo* because of the challenges of accessing and making stable recordings in the lateral horn of the spinal cord, in the thoracic region, in preparations with intact cardiorespiratory reflex function and ideally in the absence of the depressant effects of anaesthesia (for a notable exception see Dembowsky *et al.* 1986). The use of the WHBP (Paton, 1996) in combination with the slice *in situ* approach (Smith *et al.* 2007) has enabled us to obtain a view of the cellular organisation and integrative processes
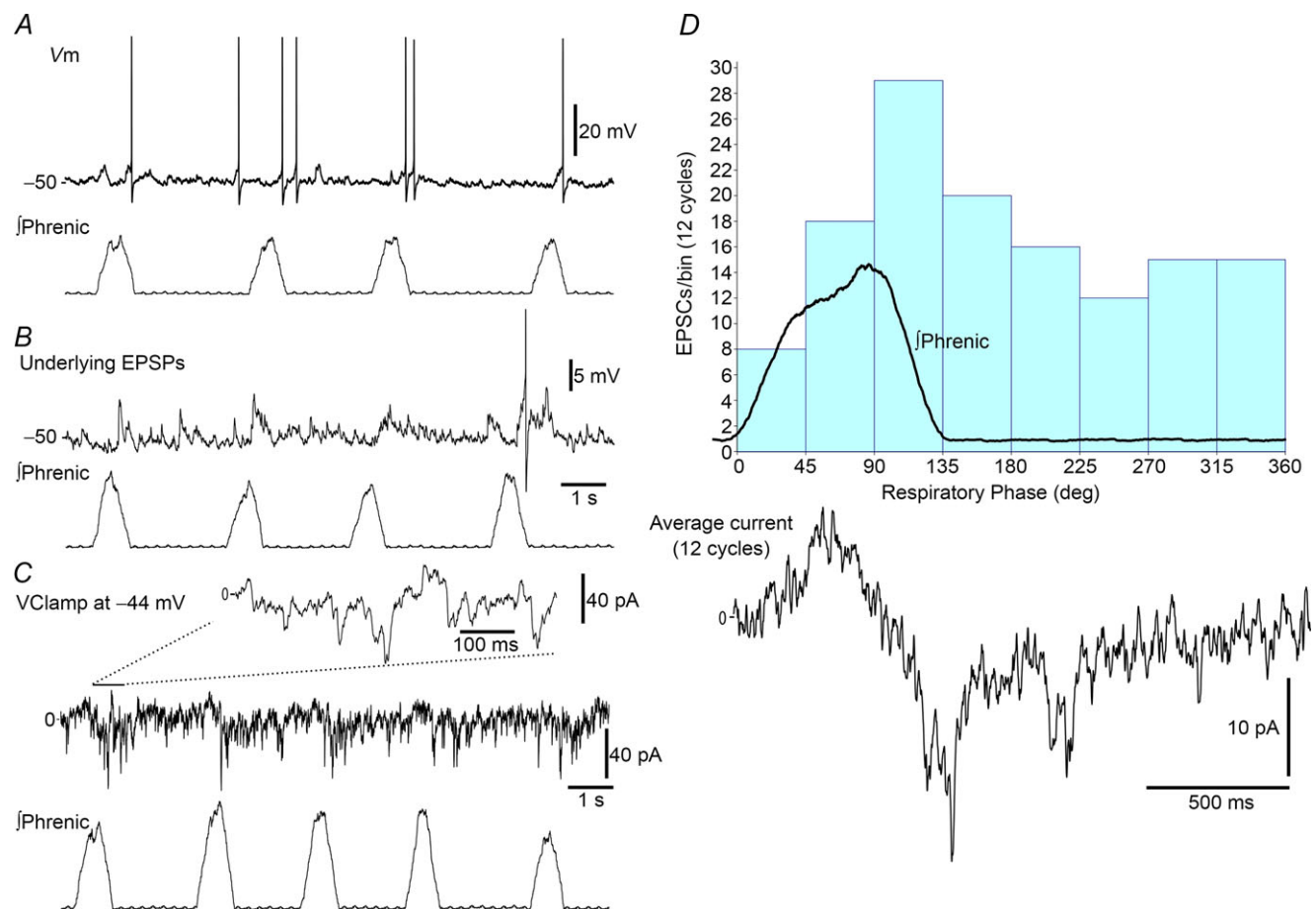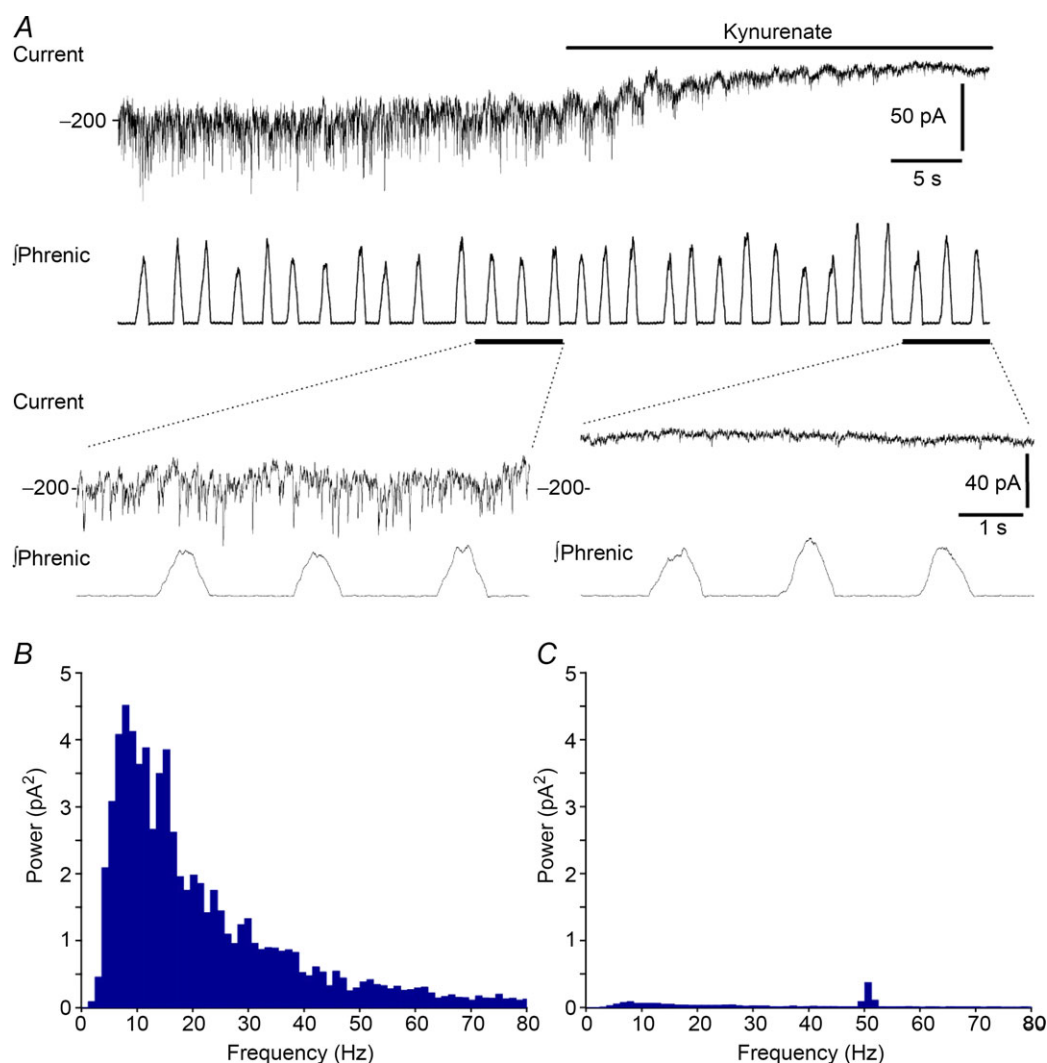

Figure 7. Synaptic drive to MVC_{like} SPNs
A, current clamp recording of spontaneous activity in an MVC_{like} SPN that had a relatively low firing frequency. The action potential discharge can be seen to fall predominantly in the post-inspiratory phase. *B*, enlarged section of the same recording showing the spontaneous EPSP activity that is arriving in the post-inspiratory phase underlying action potential discharge in the last cycle. *C*, voltage clamp of the same neurone at close to rest (-44 mV) showing the incoming barrages of EPSCs with a clear pattern of respiratory modulation. The largest events are 30–50 pA in amplitude. *D*, respiratory phase bar chart for EPSCs (amplitude >20 pA) over 12 respiratory cycles (with superimposed average phrenic waveform). This shows the grouping of these larger EPSCs into the late-I/early-PI phase. Averaging the holding current over this time period (beneath) also demonstrates this respiratory oscillation in the synaptic current of around 20 pA.

of autonomic control at the level of the SPN. Our studies were conducted on neonatal rats (aged ~10 days) as this facilitated patch clamp recording and also extended the preparation viability giving a longer time window for recordings. We have previously shown that autonomic reflex function is robustly established in the WHBP at this age (Simms *et al.* 2009) and it is worth noting that the functional organisation of the sympathetic outflow and its descending drives (although still immature) is already well differentiated in the neonate, indicating its importance as a priority homeostatic and defence system.

Intrinsic electrophysiology

Our recordings have shown that SPNs in the WHBP exhibit characteristic electrophysiological features such as: large, prolonged action potentials with a prominent shoulder on repolarisation; slow and fast AHPs; a powerful transient rectification; rebound excitations; and anomalous rectification like those that have been reported from *in vitro* studies across several species (Yoshimura *et al.* 1986*a*, 1987*a*,*b*; Spanswick & Logan, 1990*b*; Pickering *et al.* 1991; Sah & McLachlan, 1995; Miyazaki *et al.* 1996; Wilson *et al.* 2002; Zimmerman & Hochman, 2010; Whyment *et al.*


Figure 8. Excitatory amino acid-mediated synaptic drive to MVC_like SPNs
Voltage clamp recording of an MVC_like SPN showing the incoming synaptic activity with a respiratory modulated pattern (enlarged below, holding potential −80 mV, same cell as Fig. 7). Local superfusion of the broad-spectrum ionotropic excitatory amino acid receptor antagonist (50 mM) produced a block of these synaptic events (shown below) without affecting the phrenic activity indicative of localisation of drug application. Furthermore, the kynurenate blockade revealed a tonic as well as phasic component to the excitatory synaptic drive of almost 40 pA in this instance. This was also reflected in the dramatic loss of power in the current record (*B* and *C*) across the spectrum on application of kynurenate (current bandpass filtered 5–500 Hz and fast Fourier transformed with a Hanning window to 4096 bins, each bin width 1.2 Hz; note the 50 Hz peak is mains hum – clear in *C*).

2011). A notable difference, evident from our recordings, is that the resting potentials tend to be more depolarised (-52 mV) than has been found *in vitro* (average V_m ranging from -44 to -62 with a median of -59 mV

(Spanswick & Logan, 1990*a,b*; Pickering *et al.* 1991, 1994; Sah & McLachlan, 1995; Logan *et al.* 1996; Nolan *et al.* 1999; Wilson *et al.* 2002), probably as a consequence of the intact synaptic drives in the WHBP.
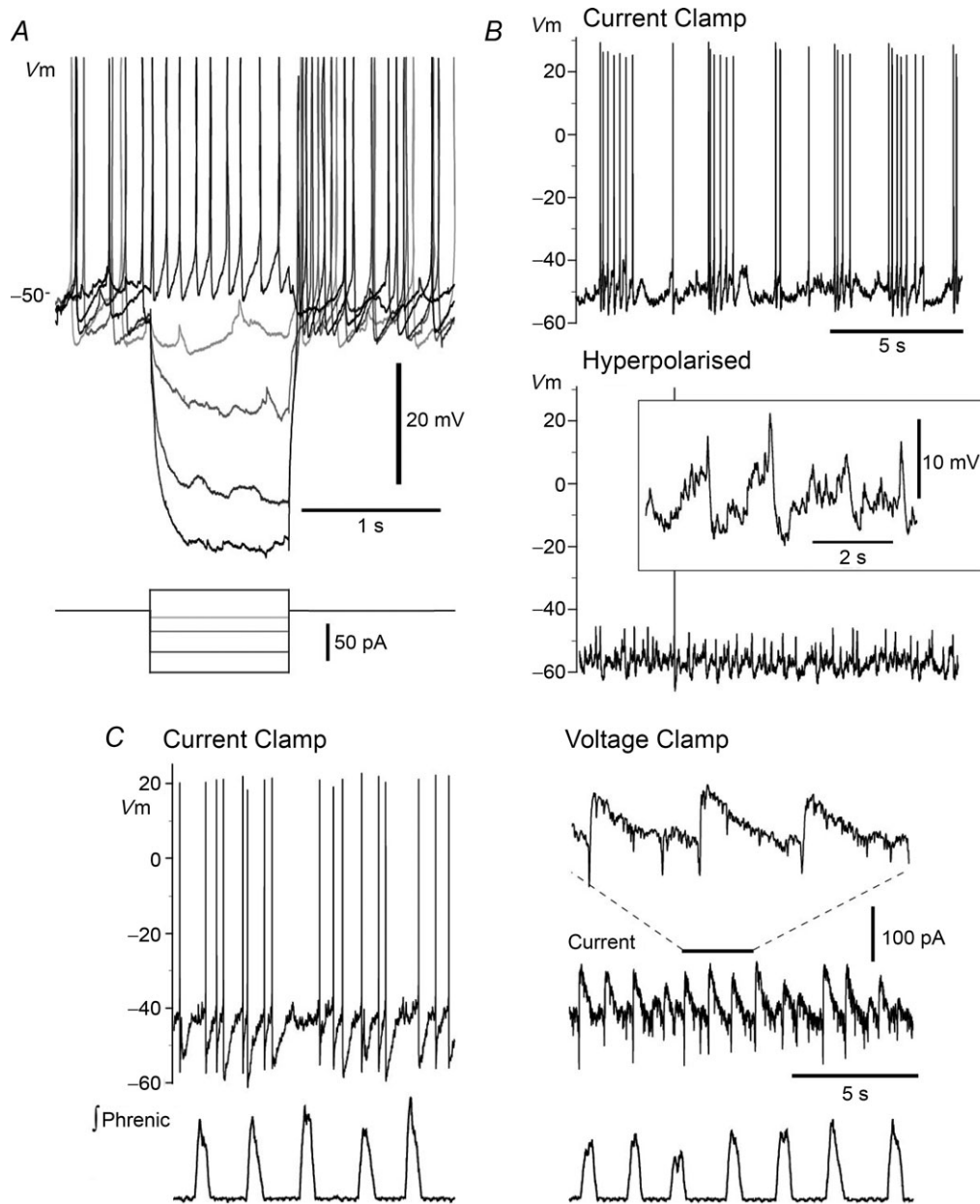
Figure 9. Characteristics of CVC$_{like}$ SPNs
A, current clamp recording of a CVC$_{like}$ SPN firing spontaneously at rest. This firing was inhibited by the injection of hyperpolarising current pulses (1 s), the cell showed a degree of anomalous rectification but there was no evidence of a transient rectification following the offset of the larger pulses, which was instead marked by a period of rebound excitation and action potential discharge. Depolarisation increased the rate of action potential discharge but this was not followed at the offset of the pulse by a slow AHP. *B*, another CVC$_{like}$ neurone showing a bursting pattern of discharge at rest. The injection of hyperpolarising current revealed the presence of biphasic rhythmical membrane potential oscillations (shown on faster timescale in the inset). *C*, current and voltage clamp recordings of another CVC$_{like}$ neurone. Clamp at a holding potential of 5 mV hyperpolarised to resting showed large biphasic current oscillations (~200 pA) that underlay the firing activity with superimposed smaller fast excitatory synaptic potentials.

Table 4. Comparison of MVC$_{like}$ and CVC$_{like}$ properties of SPNs

	MVC$_{like}$		CVC$_{like}$		
	Mean	*n*	Mean	*n*	*P*
Resting potential (mV)	-51.9 ± 0.8	38	-52.6 ± 1.0	27	0.54
Input resistance (MΩ)	495.5 ± 40.7	36	346.2 ± 49.1	23	0.024
Time constant (ms)	34.12 ± 2.6	33	31.2 ± 4.3	20	0.54
Spike frequency (Hz)	2.52 ± 0.33	38	1.34 ± 0.17	27	0.007
Spike threshold (mV)	-41.9 ± 0.8	38	-42.6 ± 0.9	27	0.51
Spike amplitude (mV)	48.4 ± 1.2	38	49.3 ± 1.9	27	0.68
Spike duration (ms)	3.69 ± 0.18	38	3.42 ± 0.13	27	0.28
AHP amplitude (mV)	-17.8 ± 0.5	38	-19.4 ± 0.8	27	0.074
AHP duration (ms)	190.7 ± 13.3	38	313.6 ± 35.8	27	<0.001

Spontaneous sympathetic activity

The majority of the SPNs (94%) in our study fired action potentials under basal conditions. The proportion of silent SPNs under basal conditions (6%) in the WHBP is considerably lower than that seen previously from high thoracic SPNs *in vivo* (45% in cat (Boczek-Funcke *et al.* 1992), 53% in rat (Gilbey *et al.* 1986), 29% in cat (Dembowsky *et al.* 1986)) or in rat thoracolumbar spinal cord slices *in vitro* (51% (Pickering *et al.* 1991), 77% (Spanswick & Logan, 1990*b*), 92% (Sah & McLachlan, 1995)). This may in part be a consequence of the intact excitatory synaptic drive in the WHBP combined with the lack of anaesthesia (known to suppress SPN activity (Logan *et al.* 1996; Nolan *et al.* 1997)) but may also partly reflect a loss of descending inhibitory control from supra-tentorial structures. Additionally, the lack of pulse wave in the WHBP means that there will be less phasic baroreflex inhibition, although the baroreceptor reflex is still active and not completely unloaded (Simms *et al.* 2007). Another likely influence is the impact of temperature of the preparation (32°C), which would be anticipated to increase the activity of a subgroup of thermoregulatory SPNs that are typically silent in the euthermic range (Morrison *et al.* 2008).

Classification of SPNs on the basis of cardiorespiratory reflex-evoked responses

We have tested the principle that it is possible to classify the 'intracellularly' recorded SPNs on the basis of their response to activation of defined cardiorespiratory afferents in the WHBP: peripheral chemoreflex afferents from the carotid body, naso-trigeminal afferents to trigger the diving response and arterial baro-afferents in the aortic depressor nerve (Paton, 1996; Dutschmann & Paton, 2002; Pickering *et al.* 2002; Braga *et al.* 2007; Simms *et al.* 2007). As we anticipated, based on the work of

Janig & Habler (2003) and Janig (2006), these stimuli have allowed the subdivisions of our population into MVC$_{like}$ (39%) and CVC$_{like}$ (28%) SPNs along with several other subgroups (discussed below). The proportions of these two main classes of SPNs is remarkably similar to the proportions previously documented in cat SPNs projecting in the cervical trunk (Boczek-Funcke *et al.* 1992) with 41% class I (proposed to be MVC-type) and 23% class 2 (CVC-type). Importantly, these subdivisions are also reflected in distinct intrinsic properties of the neurones and in their basal pattern of firing activity.

Characteristics of putative muscle vasoconstrictor SPNs

We were able to identify a population of MVC$_{like}$ neurones on the basis of their excitatory response to peripheral chemoreflex and diving response activation and their inhibition by activation of arterial baroreflex afferents (Janig & Habler, 2003). These MVC$_{like}$ neurones showed ongoing discharge under basal conditions with a characteristic pattern of respiratory modulation; the peak of activity was typically seen in the late-I to early post-I phase in line with sympathetic nerve recordings in the WHBP (Simms *et al.* 2009, 2010) and previous *in vivo* recordings (Habler *et al.* 1994). In this regard it is important to note that this respiratory–SPN coupling in the WHBP is from a central rather than peripheral source as there is no phasically varying input from pulmonary stretch receptors or from the cyclical loading of the baroreceptor afferents reflecting changes in venous return with respiration.

The activity in MVC$_{like}$ SPNs was driven by summing bursts of EPSPs and there was a continuous sub-threshold synaptic barrage arriving at these neurones. This synaptic drive was sensitive to spinal kynurenate application (indicating the involvement of excitatory amino acid receptors), which has previously been shown

to block tonic and rostral ventrolateral medulla (RVLM) stimulation-evoked sympathetic activation (Mills *et al.* 1988; Verberne *et al.* 1990; Deuchars *et al.* 1995; Morrison, 2003). This synaptic drive had both a tonic and a respiratory modulated component, the latter in phase with the peak of action potential discharge. The tonic level of excitatory synaptic drive to MVC$_{like}$ SPNs is equivalent to ∼10 mV depolarisation and probably accounts for the difference in resting potential between *in vitro* slice preparations and our *in situ* recordings. It is noteworthy that there was no evidence of a large amplitude 'dominant' synaptic input as has been seen in the pre- to post-ganglionic sympathetic synapse (McLachlan *et al.* 1998; Bratton *et al.* 2010). Based on voltage clamp studies, we were able to reliably resolve moderately large synaptic inputs that appear to underpin spike discharge (>20 pA above the baseline) and estimate that they are arriving at a rate of ∼20 Hz and that this is translated into the final spike discharge rate of ∼2 Hz. The MVC$_{like}$ SPNs would be silent without this drive and these observations reinforce the principle that these SPNs are indeed acting as dynamic integrators of a high frequency excitatory synaptic barrage.

Given the bandwidth step-down being performed by the MVC$_{like}$ SPNs (in turning a high frequency synaptic drive (>20 Hz) into a low frequency action potential output (∼2 Hz)), their intrinsic properties are of considerable importance in determining the outputs of this autonomic neural calculation. In this respect, the MVC$_{like}$ SPNs have the prototypical characteristic features previously reported from *in vitro* studies of SPNs with fast and slow AHPs and a strong transient rectification, all of which may be modulated to powerfully regulate the pattern of spike discharge. The influence of these integrative properties on sympathetic outflow have been illustrated by a study using optogenetic stimulation of C1 neurones in the RVLM, which showed marked paired pulse depression of the sympathetic excitatory response to each brainstem activation (Abbott *et al.* 2009). The authors concluded that this probably reflected the rectifying properties of the SPN, something that has been reported from recordings in the isolated spinal cord (McKenna & Schramm, 1985) and intriguingly this has been linked to the sympathetic over-activity seen in the spontaneously hypertensive rat (Schramm & Barton, 1979).

The respiratory modulated component of the synaptic drive to the MVC$_{like}$ SPNs gives rise to the pattern of respiratory-related activity recorded on many sympathetic nerves (Adrian *et al.* 1932; Habler *et al.* 1994). This respiratory coupling of MVC$_{like}$ discharge was amplified and concentrated during peripheral chemoreflex activation such that the additional firing was predominantly seen in the late I/early-PI period. This indicates that rather than just having a tonic increase in their activity across all phases of the respiratory cycle, these SPNs are receiving synaptic inputs from a population of neurones that provides a specific drive in the late-I/early-PI phase. This may give a clue as to the origin of the synaptic drive from the peripheral chemoreflex to these SPNs, and some subsets of neurones within the RVLM are reported to have this pattern of discharge (Guyenet, 2000), are activated by the peripheral chemoreflex (Koshiya & Guyenet, 1996) and act by a monosynaptic excitatory amino acid-mediated drive to SPNs (Morrison, 2003).

Our classification of these SPNs as MVC$_{like}$ is undoubtedly a simplification and given the recording location at T3–4 they are likely to include some visceral vasomotor neurones as well some of the cardiac sympathetic neurones (Strack *et al.* 1989; Anderson *et al.* 2009), which would both be expected to be excited by activation of the peripheral chemoreflex and diving response and inhibited by baroafferent stimulation (see Paton *et al.* 2005). As yet, no obvious differential characteristic has emerged amongst the group of MVC$_{like}$ SPNs either in terms of their intrinsic characteristics or in terms of their patterns of activity under basal conditions or during reflex activation. It may be possible to combine our recording methodology with *post hoc* neurochemical analysis (Gonsalvez *et al.* 2010) to attempt to further subdivide the MVC$_{like}$ SPNs.

Characteristics of putative cutaneous vasoconstrictor SPNs

We identified the CVC$_{like}$ SPNs on the basis of their characteristically strong inhibitory responses to both peripheral chemoreflex activation and the diving response. These fired slower than the MVC$_{like}$ SPNs and showed a reciprocal pattern of respiratory modulation with a nadir in late-I/early-PI as reported before for CVCs innervating the rat tail (Habler *et al.* 1999). Two of these CVC$_{like}$ SPNs were also clearly inhibited by noxious pinch of the ipsilateral forepaw – constituting the Lovén reflex – reinforcing their functional identification (not routinely tested because of risk of losing recording; data not shown).

The activity of the CVC$_{like}$ SPNs was driven by rhythmical biphasic membrane potential oscillations that have previously been documented in SPNs *in vitro* (Spanswick & Logan, 1990*a*; Pickering *et al.* 1994; Logan *et al.* 1996; Nolan *et al.* 1999). This has been shown to result from electrotonic coupling between SPNs. This rhythmical activity was not seen in any of the MVC$_{like}$ SPNs, indicating that it is likely to be a functional specialisation that is specific to the role of the CVC$_{like}$ SPNs. The presence of the electrotonic coupling between CVC$_{like}$ SPNs also accounts in part for their lower input resistances and longer AHPs than the MVC$_{like}$ SPNs. Although our recordings were obtained from neonatal (P5–16) WHBPs it is apparent that the patterns of activity, both spontaneous and reflex-evoked, were entirely comparable to those

documented in adult rats *in vivo* (Habler *et al.* 1999). It may be that the presence of gap junctional coupling in these neurones could be a developmental phenomenon but we noted no reduction in the proportions of CVC$_{like}$ neurones showing oscillations with age (22% P5–8; 30% P9–12; 41% P13–16). Additionally, the gap junctional coupling between SPNs *in vitro* has also been reported in adult rat spinal cord (Leslie *et al.* 2000; D. Spanswick, personal communication).

Given their opposing responses to reflex activation and mirror image pattern of respiratory modulation, the CVC$_{like}$ SPNs must also receive a different pattern of synaptic drive compared to the MVC$_{like}$ SPNs. Only around a half of the CVC$_{like}$ SPNs expressed the characteristic transient or anomalous rectification and the slow AHP – and these were typically expressed in concert. Similarly, only a minority were inhibited by aortic depressor nerve activation and this was weaker than the effect on MVC$_{like}$ neurones. From the foregoing it is apparent that there are distinctive characteristics of CVC$_{like}$ neurones in terms of their intrinsic properties, network connectivity, potential subgroups and synaptic drives.

In summary, we have been able to relate the intrinsic electrophysiological properties of several classes of SPNs to their function in mediating cardiorespiratory reflexes and uncover some of the distinctive principles by which they integrate their patterns of spontaneous and reflex-evoked synaptic input. This has revealed discrete cellular and network behaviours of the neurones that is likely to be related to their functional specialisation. In the case of the MVC$_{like}$ neurones this has allowed us to characterise the synaptic input that underpins the generation and flux of sympathetic tone to the periphery and more generally has emphasised both the differences in and the importance of the intrinsic membrane properties of distinct classes of SPNs in the integration of these complex drives.

References

Abbott SB, Stornetta RL, Socolovsky CS, West GH & Guyenet PG (2009). Photostimulation of channelrhodopsin-2 expressing ventrolateral medullary neurons increases sympathetic nerve activity and blood pressure in rats. *J Physiol* **587**, 5613–5631.

Adrian ED, Bronk DW & Phillips G (1932). Discharges in mammalian sympathetic nerves. *J Physiol* **74**, 115–133.

Anderson C, Keast J & McLachlan E (2009). Spinal autonomic preganglionic neurons: the visceral efferent system of the spinal cord. In *The Spinal Cord*, ed. Watson C, Paxinos G & Kayalioglu G, pp. 115–129. Elsevier, London.

Boczek-Funcke A, Dembowsky K, Habler HJ, Janig W, McAllen RM & Michaelis M (1992). Classification of preganglionic neurones projecting into the cat cervical sympathetic trunk. *J Physiol* **453**, 319–339.

Braga VA, Soriano RN, Braccialli AL, de Paula PM, Bonagamba LG, Paton JF & Machado BH (2007). Involvement of L-glutamate and ATP in the neurotransmission of the sympathoexcitatory component of the chemoreflex in the commissural nucleus tractus solitarii of awake rats and in the working heart–brainstem preparation. *J Physiol* **581**, 1129–1145.

Bratton BO, Davies P, Janig W & McAllen RM (2010). Ganglionic transmission in a vasomotor pathway studied *in vivo*. *J Physiol* **588**, 1647–1659.

Coote JH (1988). The organisation of cardiovascular neurons in the spinal cord. *Rev Physiol Biochem Pharmacol* **110**, 147–285.

Coote JH & Westbury DR (1979). Intracellular recordings from sympathetic preganglionic neurones. *Neurosci Lett* **15**, 171–175.

Dampney RA & McAllen RM (1988). Differential control of sympathetic fibres supplying hindlimb skin and muscle by subretrofacial neurones in the cat. *J Physiol* **395**, 41–56.

Dembowsky K, Czachurski J & Seller H (1986). Three types of sympathetic preganglionic neurones with different electrophysiological properties are identified by intracellular recordings in the cat. *Pflugers Arch* **406**, 112–120.

Deuchars SA, Morrison SF & Gilbey MP (1995). Medullary-evoked EPSPs in neonatal rat sympathetic preganglionic neurones *in vitro*. *J Physiol* **487**, 453–463.

Dutschmann M & Paton JF (2002). Influence of nasotrigeminal afferents on medullary respiratory neurones and upper airway patency in the rat. *Pflugers Arch* **444**, 227–235.

Esler M (2011). The sympathetic nervous system through the ages: from Thomas Willis to resistant hypertension. *Exp Physiol* **96**, 611–622.

Fernandez de Molina A, Kuno M & Perl ER (1965). Antidromically evoked responses from sympathetic preganglionic neurones. *J Physiol* **180**, 321–335.

Fisher JP & Paton JF (2012). The sympathetic nervous system and blood pressure in humans: implications for hypertension. *J Hum Hypertens* **26**, 463–475.

Gilbey MP, Numao Y & Spyer KM (1986). Discharge patterns of cervical sympathetic preganglionic neurones related to central respiratory drive in the rat. *J Physiol* **378**, 253–265.

Gonsalvez DG, Kerman IA, McAllen RM & Anderson CR (2010). Chemical coding for cardiovascular sympathetic preganglionic neurons in rats. *J Neurosci* **30**, 11781–11791.

Guyenet PG (2000). Neural structures that mediate sympathoexcitation during hypoxia. *Respir Physiol* **121**, 147–162.

Guyenet PG (2006). The sympathetic control of blood pressure. *Nat Rev Neurosci* **7**, 335–346.

Habler H, Bartsch T & Janig W (1999). Rhythmicity in single fiber postganglionic activity supplying the rat tail. *J Neurophysiol* **81**, 2026–2036.

Habler HJ, Janig W & Michaelis M (1994). Respiratory modulation in the activity of sympathetic neurones. *Prog Neurobiol* **43**, 567–606.

Janig W (2006). *The Integrative Action of the Autonomic Nervous System*. Cambridge University Press, Cambridge.

Janig W & Habler HJ (2003). Neurophysiological analysis of target-related sympathetic pathways–from animal to human: similarities and differences. *Acta Physiol Scand* **177**, 255–274.

Koshiya N & Guyenet PG (1996). Tonic sympathetic chemoreflex after blockade of respiratory rhythmogenesis in the rat. *J Physiol* **491**, 859–869.

Leslie J, Nolan MF, Logan SD & Spanswick D (2000). Electrotonic coupling between sympathetic preganglionic neurones in neonatal and adult rat, *in vitro*. *J Physiol* **528**, 108P.

Logan SD, Pickering AE, Gibson IC, Nolan MF & Spanswick D (1996). Electrotonic coupling between rat sympathetic preganglionic neurones *in vitro*. *J Physiol* **495**, 491–502.

Malpas SC (2010). Sympathetic nervous system overactivity and its role in the development of cardiovascular disease. *Physiol Rev* **90**, 513–557.

McBryde FD, Abdala AP, Hendy EB, Pijacka W, Marvar P, Moraes DJ, Sobotka PA & Paton JF (2013). The carotid body as a putative therapeutic target for the treatment of neurogenic hypertension. *Nat Commun* **4**, 2395.

McKenna KE & Schramm LP (1985). Mechanisms mediating the sympathetic silent period: studies in the isolated spinal cord of the neonatal rat. *Brain Res* **329**, 233–240.

McLachlan EM, Habler HJ, Jamieson J & Davies PJ (1998). Analysis of the periodicity of synaptic events in neurones in the superior cervical ganglion of anaesthetized rats. *J Physiol* **511**, 461–478.

McLachlan EM & Hirst GD (1980). Some properties of preganglionic neurons in upper thoracic spinal cord of the cat. *J Neurophysiol* **43**, 1251–1265.

Mills EH, Minson JB, Pilowsky PM & Chalmers JP (1988). N-methyl-D-aspartate receptors in the spinal cord mediate pressor responses to stimulation of the rostral ventrolateral medulla in the rat. *Clin Exp Pharmacol Physiol* **15**, 147–155.

Miyazaki T, Dun NJ, Kobayashi H & Tosaka T (1996). Voltage-dependent potassium currents of sympathetic preganglionic neurons in neonatal rat spinal cord thin slices. *Brain Res* **743**, 1–10.

Morrison SF (2001). Differential control of sympathetic outflow. *Am J Physiol Regul Integr Comp Physiol* **281**, R683–698.

Morrison SF (2003). Glutamate transmission in the rostral ventrolateral medullary sympathetic premotor pathway. *Cell Mol Neurobiol* **23**, 761–772.

Morrison SF & Cao WH (2000). Different adrenal sympathetic preganglionic neurons regulate epinephrine and norepinephrine secretion. *Am J Physiol Regul Integr Comp Physiol* **279**, R1763–R1775.

Morrison SF, Nakamura K & Madden CJ (2008). Central control of thermogenesis in mammals. *Exp Physiol* **93**, 773–797.

Nolan MF, Gibson IC & Logan SD (1997). Actions of the anaesthetic Saffan on rat sympathetic preganglionic neurones *in vitro*. *Br J Pharmacol* **121**, 324–330.

Nolan MF, Logan SD & Spanswick D (1999). Electrophysiological properties of electrical synapses between rat sympathetic preganglionic neurones *in vitro*. *J Physiol* **519**, 753–764.

Paton JF (1996). A working heart–brainstem preparation of the mouse. *J Neurosci Methods* **65**, 63–68.

Paton JF, Boscan P, Pickering AE & Nalivaiko E (2005). The yin and yang of cardiac autonomic control: vago-sympathetic interactions revisited. *Brain Res Rev* **49**, 555–565.

Pickering AE, Spanswick D & Logan SD (1991). Whole-cell recordings from sympathetic preganglionic neurons in rat spinal cord slices. *Neurosci Lett* **130**, 237–242.

Pickering AE, Spanswick D & Logan SD (1994). 5-Hydroxytryptamine evokes depolarizations and membrane potential oscillations in rat sympathetic preganglionic neurones. *J Physiol* **480**, 109–121.

Pickering AE, Waki H, Headley PM & Paton JF (2002). Investigation of systemic bupivacaine toxicity using the *in situ* perfused working heart–brainstem preparation of the rat. *Anesthesiology* **97**, 1550–1556.

Polosa C, Yoshimura M & Nishi S (1988). Electrophysiological properties of sympathetic preganglionic neurons. *Annu Rev Physiol* **50**, 541–551.

Robertson D, Biaggioni I, Burnstock G, Low P & Paton J, ed (2012). *Primer on the Autonomic Nervous System*. Academic Press, New York.

Sah P & McLachlan EM (1995). Membrane properties and synaptic potentials in rat sympathetic preganglionic neurons studied in horizontal spinal cord slices in vitro. *J Auton Nerv Syst* **53**, 1–15.

Schramm LP & Barton GN (1979). Diminished sympathetic silent period in spontaneously hypertensive rats. *Am J Physiol* **236**, R147–R152.

Simms AE, Paton JF, Allen AM & Pickering AE (2010). Is augmented central respiratory–sympathetic coupling involved in the generation of hypertension? *Respir Physiol Neurobiol* **174**, 89–97.

Simms AE, Paton JF & Pickering AE (2007). Hierarchical recruitment of the sympathetic and parasympathetic limbs of the baroreflex in normotensive and spontaneously hypertensive rats. *J Physiol* **579**, 473–486.

Simms AE, Paton JF, Pickering AE & Allen AM (2009). Amplified respiratory–sympathetic coupling in the spontaneously hypertensive rat: does it contribute to hypertension? *J Physiol* **587**, 597–610.

Smith JC, Abdala AP, Koizumi H, Rybak IA & Paton JF (2007). Spatial and functional architecture of the mammalian brain stem respiratory network: a hierarchy of three oscillatory mechanisms. *J Neurophysiol* **98**, 3370–3387.

Spanswick D & Logan SD (1990*a*). Spontaneous rhythmic activity in the intermediolateral cell nucleus of the neonate rat thoracolumbar spinal cord *in vitro*. *Neuroscience* **39**, 395–403.

Spanswick D & Logan SD (1990*b*). Sympathetic preganglionic neurones in neonatal rat spinal cord *in vitro*: electrophysiological characteristics and the effects of selective excitatory amino acid receptor agonists. *Brain Res* **525**, 181–188.

Strack AM, Sawyer WB, Hughes JH, Platt KB & Loewy AD (1989). A general pattern of CNS innervation of the sympathetic outflow demonstrated by transneuronal pseudorabies viral infections. *Brain Res* **491**, 156–162.

Verberne AJ, Widdop RE, Maccarrone C, Jarrott B, Beart PM & Louis WJ (1990). Intrathecal kynurenate reduces arterial pressure, heart rate and baroreceptor–heart rate reflex in conscious rats. *Neurosci Lett* **114**, 309–315.

Whyment AD, Coderre E, Wilson JM, Renaud LP, O'Hare E & Spanswick D (2011). Electrophysiological, pharmacological and molecular profile of the transiently outward rectifying conductance in rat sympathetic preganglionic neurons *in vitro*. *Neuroscience* **178**, 68–81.

Wilson JM, Coderre E, Renaud LP & Spanswick D (2002). Active and passive membrane properties of rat sympathetic preganglionic neurones innervating the adrenal medulla. *J Physiol* **545**, 945–960.

Yoshimura M, Polosa C & Nishi S (1986*a*). Afterhyperpolarization mechanisms in cat sympathetic preganglionic neuron *in vitro*. *J Neurophysiol* **55**, 1234–1246.

Yoshimura M, Polosa C & Nishi S (1986*b*). Electrophysiological properties of sympathetic preganglionic neurons in the cat spinal cord *in vitro*. *Pflugers Arch* **406**, 91–98.

Yoshimura M, Polosa C & Nishi S (1987*a*). Afterdepolarization mechanism in the *in vitro*, cesium-loaded, sympathetic preganglionic neuron of the cat. *J Neurophysiol* **57**, 1325–1337.

Yoshimura M, Polosa C & Nishi S (1987*b*). A transient outward rectification in the cat sympathetic preganglionic neuron. *Pflugers Arch* **408**, 207–208.

Zimmerman A & Hochman S (2010). Heterogeneity of membrane properties in sympathetic preganglionic neurons of neonatal mice: evidence of four subpopulations in the intermediolateral nucleus. *J Neurophysiol* **103**, 490–498.

Zoccal DB, Simms AE, Bonagamba LG, Braga VA, Pickering AE, Paton JF & Machado BH (2008). Increased sympathetic outflow in juvenile rats submitted to chronic intermittent hypoxia correlates with enhanced expiratory activity. *J Physiol* **586**, 3253–3265.

Additional information

Competing interests

The authors have no competing interests to declare.

Author contributions

The experiments were performed in the Pickering lab. A.E.P., J.F.R.P. and A.O.S. conceived and designed the experiments. A.O.S. collected the experimental data and all authors contributed to analysis and interpretation. All authors contributed to drafting the article. All authors have approved the final version of the manuscript, all persons designated as authors qualify for authorship, and all those who qualify for authorship are listed.